Monthly Notices
of the
ROYAL ASTRONOMICAL SOCIETY

MNRAS **465,** 2833–2848 (2017)
Advance Access publication 2016 November 3

doi:10.1093/mnras/stw2826

The evolution of the galaxy content of dark matter haloes

S. Contreras,[1,2⋆] I. Zehavi,[3,2⋆] C. M. Baugh,[2] N. Padilla[1,4] and P. Norberg[2,5]

[1]*Institúto Astrofísica, Pontifica Universidad Católica de Chile, 7820436 Santiago, Chile*
[2]*Institute for Computational Cosmology, Department of Physics, Durham University, South Road, Durham DH1 3LE, UK*
[3]*Department of Astronomy, Case Western Reserve University, Cleveland, OH 44106, USA*
[4]*Centro de Astro-Ingeniería, Pontificia Universidad Católica de Chile, 7820436 Santiago, Chile*
[5]*Centre for Extragalactic Astronomy, Department of Physics, Durham University, South Road, Durham DH1 3LE, UK*

Accepted 2016 November 1. Received 2016 October 30; in original form 2016 July 20

ABSTRACT

We use the halo occupation distribution (HOD) framework to characterize the predictions from two independent galaxy formation models for the galactic content of dark matter haloes and its evolution with redshift. Our galaxy samples correspond to a range of fixed number densities defined by stellar mass and span $0 \leq z \leq 3$. We find remarkable similarities between the model predictions. Differences arise at low galaxy number densities which are sensitive to the treatment of heating of the hot halo by active galactic nuclei. The evolution of the form of the HOD can be described in a relatively simple way, and we model each HOD parameter using its value at $z = 0$ and an additional evolutionary parameter. In particular, we find that the ratio between the characteristic halo masses for hosting central and satellite galaxies can serve as a sensitive diagnostic for galaxy evolution models. Our results can be used to test and develop empirical studies of galaxy evolution, and can facilitate the construction of mock galaxy catalogues for future surveys.

Key words: galaxies: evolution – galaxies: haloes – galaxies: statistics – cosmology: theory – large-scale structure of Universe.

1 INTRODUCTION

In the standard cosmological framework, galaxies form, evolve and reside in dark matter haloes. A key requirement of this framework is to understand how galaxies populate dark matter haloes. What determines how many galaxies are hosted by a dark matter halo? How do the properties of galaxies depend on the mass of the halo? These questions lie at the core of galaxy formation theory. The answers are also crucial if we are to take full advantage of the next generation of galaxy surveys, which aim to make pristine clustering measurements to pin down the nature of dark energy. The extraction of cosmological inferences from these data will no longer be dominated by statistical errors but instead will be limited by the accuracy of our theoretical models. Understanding how galaxies relate to the underlying dark matter is thus essential for optimally utilizing the large-scale distribution of galaxies as a cosmological probe.

The clustering of dark matter is dominated by gravity and can be computed reliably with cosmological *N*-body simulations. However, the detailed physics of galaxy formation – gas cooling, star formation and feedback effects – is only partially understood, so that the relation between galaxies and the underlying dark matter cannot be predicted robustly from first principles.

A useful approach to study this is semi-analytic modeling of galaxy formation (for reviews, see e.g. Cole et al. 2000; Baugh 2006; Benson 2010; Somerville & Davé 2015). In such models, haloes identified in *N*-body simulations are 'populated' with galaxies using analytical prescriptions for the baryonic processes. Following the dark matter merger trees, galaxies merge and evolve as new stars form and previous generations of stars change. Different feedback or heating mechanisms, such as those caused by star formation, active galactic nuclei, or the photoionizing ultraviolet background, are also incorporated. Semi-analytic models (SAMs) have been successful in reproducing a range of observed properties including stellar mass functions and galaxy luminosity functions (see e.g. Bower et al. 2006; Croton et al. 2006; Fontanot et al. 2009; Guo et al. 2011, 2013; Gonzalez-Perez et al. 2014; Padilla et al. 2014; Henriques et al. 2015; Croton et al. 2016; Lacey et al. 2016).

The connection between the mass of a dark matter halo and the galaxies which populate it is often expressed through the halo occupation distribution (HOD) framework (e.g. Jing, Mo & Börner 1998; Benson et al. 2000; Peacock & Smith 2000; Seljak 2000; Scoccimarro et al. 2001; Berlind & Weinberg 2002; Cooray & Sheth 2002; Berlind et al. 2003; Yang, Mo & van den Bosch 2003; Kravtsov et al. 2004; Zheng et al. 2005; Conroy, Wechsler & Kravtsov 2006). The HOD formalism describes the 'bias' relation between galaxies and mass at the level of individual dark matter haloes, in terms

⋆ E-mail: stcontre@uc.cl (SC); idit.zehavi@case.edu (IZ)

of the probability distribution that a halo of virial mass $M_{\rm h}$ contains N galaxies which satisfy a particular selection criterion. It transforms measures of galaxy clustering into a physical relation between galaxies and dark matter haloes, setting the stage for detailed tests of galaxy formation models. The HOD approach has proven to be a very powerful theoretical tool to constrain the galaxy–halo connection and has been applied to interpret clustering data from numerous surveys at low and high redshifts (e.g. Jing & Börner 1998; Bullock, Wechsler & Somerville 2002; Jing, Börner & Suto 2002; Moustakas & Somerville 2002; Magliocchetti & Porciani 2003; van den Bosch, Yang & Mo 2003; Yan, Madgwick & White 2003; Zheng 2004; Yang et al. 2005; Zehavi et al. 2005, 2011; Cooray 2006; Hamana et al. 2006; Lee et al. 2006, 2009; Phleps et al. 2006; White et al. 2007, 2011; Zheng, Coil & Zehavi 2007; Blake, Collister & Lahav 2008; Brown et al. 2008; Quadri et al. 2008; Wake et al. 2008, 2011; Kim et al. 2009; Simon et al. 2009; Zheng et al. 2009; Ross, Percival & Brunner 2010; Coupon et al. 2012, 2015; de la Torre et al. 2013; Krause et al. 2013; Parejko et al. 2013; Guo et al. 2014; Durkalec et al. 2015; Kim et al. 2015; McCracken et al. 2015; Skibba et al. 2015).

HOD models have mostly been used to constrain the relation between galaxies and haloes at a fixed epoch, as the HOD approach by itself does not offer any guidance as to how to treat the evolution of the galaxy population over cosmic time. Attempts to study galaxy evolution using this framework have, for the most part, explored 'snapshots' of clustering at different epochs to empirically constrain the evolution (e.g. White et al. 2007; Zheng et al. 2007; Wake et al. 2008, 2011; Abbas et al. 2010; Coupon et al. 2012; de la Torre et al. 2013; Guo et al. 2014; Manera et al. 2015; Skibba et al. 2015), but a complete model for the evolution of the HOD is still missing.

Our goal is to remedy this situation and develop a theoretical model for this evolution by studying how the HOD changes with time. A simplified approach in this vein was taken by Seo, Eisenstein & Zehavi (2008), who studied the predictions for passive evolution of the HOD by populating simulations with galaxies according to a range of assumed HOD and tracking their evolution with time. That work is of limited use due to the unphysical assumption of passive evolution. The form of the HOD at different redshifts has also been studied in the context of abundance matching modelling (Kravtsov et al. 2004; Conroy et al. 2006). Here, we will perform a comprehensive study of the evolution of the HOD using the predictions of SAM which captures the important galaxy formation physics.

This paper builds upon our work exploring the predictions of SAM of galaxy formation, focusing on the connection between galaxies and their host dark matter haloes. Contreras et al. (2013) demonstrated that SAMs from different groups give consistent predictions for the galaxy correlation function on large scales, for samples constructed to have the same abundance of galaxies, and that the differences on small scales (the so-called one-halo term) can be readily understood in terms of the choices made about the placement of galaxies within dark matter haloes. In a second paper, we examined the connection between different galaxy properties and the mass of the dark matter halo hosting the galaxy (Contreras et al. 2015). We found that some properties, such as stellar mass, depend on subhalo mass in a monotonic fashion (albeit with a scatter), whereas others, such as the cold gas mass, have a more complex dependence on halo mass.

Here, we use the HOD formalism to compare how different models populate haloes with galaxies over cosmic time. We study the output of two independently developed SAMs, originally from the Durham and Munich groups, at different number densities. This allows us to assess which features of the predicted HODs are generic and which are sensitive to the details of the modelling of the various physical processes, and how best to describe the evolution of the HOD at a given number density. We also consider some simplified empirical models for the evolution of the galaxy distribution and show how these differ from the predictions of the SAMs.

This study will enable the incorporation of evolution into the halo models, an aspect that is absent from the standard implementation. The applications of this are twofold. First, from the observational side, it will allow for a consistent combined analysis of clustering measures over a range of epochs, in order to constrain galaxy formation and evolution. A second application of the HOD is to quantify evolution in the galaxy population, which will facilitate the creation of realistic mock galaxy catalogues for surveys which span a large range of lookback times. Accurate estimates exist for the form of the HOD using measurements of the galaxy clustering in, for example, local surveys (e.g. Zehavi et al. 2011). These can be used, in conjunction with a sample of dark matter haloes extracted from an N-body simulation to build a mock catalogue with the same clustering properties and abundance of galaxies. The problem then is how to extend this approach to build a catalogue that expands beyond the redshift interval covered by the original survey, for use with upcoming surveys. Our evolution study presented here is an essential input for such efforts.

The outline of this paper is as follows: in Section 2, we introduce the SAMs used, along with the N-body simulation the models are grafted on to, and we describe the HOD characterization of the galaxy population. In Section 3, we show the evolution of the HODs for a wide range of number densities and redshifts, we fit the HODs predicted by the SAMs and we show the evolution of the best-fitting parameters. In Section 4, we compare our results with simple models for the evolution of galaxy clustering. Finally, in Section 5, we present our conclusions.

2 MODELS OF GALAXY CLUSTERING

Here, we review the different galaxy formation models used (Section 2.1) and outline the HOD description of the way in which dark matter haloes are populated by galaxies (Section 2.2).

2.1 Galaxy formation models

We first give a brief overview of the galaxy formation models we use (Section 2.1.1). We then provide the details of the N-body simulation they are implemented in, and outline the construction of the halo merger trees and reconcile the different halo mass definition used by the groups of modellers (Section 2.1.2).

2.1.1 The SAMs

The objective of SAMs is to model the main physical processes involved in the evolution and formation of galaxies. Some of these processes are: collapse and merging of dark matter haloes; shock heating and radiative cooling of gas; star formation; supernovae, AGN and photoionization feedback; chemical enrichment of gas and stars; disc instability; and galaxy mergers.

We chose SAMs that have different implementations of these processes, so that we can identify which results are robust and which ones depend on the physical treatment in the models.

The SAMs we use are those of (Guo et al. 2013, hereafter G13) and (Gonzalez-Perez et al. 2014, hereafter GP14).[1] The G13 model is a version of L-GALAXIES, the SAM code of the Munich group (De Lucia, Kauffmann & White 2004; Croton et al. 2006; De Lucia & Blaizot 2007; Guo et al. 2011; Henriques et al. 2013, 2015). The GP14 model is a version of GALFORM, developed by the Durham group (Bower et al. 2006; Font et al. 2008; Lagos et al. 2012; Lacey et al. 2016). The GP14 model has an improved treatment of star formation, dividing the interstellar medium into molecular and atomic hydrogen components (which was introduced by Lagos et al. 2011). An important improvement of G13 and GP14 over their immediate predecessors (Guo et al. 2011; Lagos et al. 2012, respectively) is the use of a recent cosmological simulation with an updated cosmology (specified below). One notable difference between the G13 and GP14 models is the treatment of satellite galaxies. In GP14, a galaxy is assumed to lose all its hot gas halo and start decaying on to the central galaxy once it becomes a satellite. In G13, these processes are more gradual and depend on the orbit of the satellite and the destruction of the subhalo (Font et al. 2008).

2.1.2 *The Millennium simulations and halo merger trees*

The SAMs we consider are implemented in the same *N*-body simulation, the Millennium-*WMAP*7 run (hereafter MS7; G13; GP14) which is similar to the original Millennium simulation (Springel et al. 2005) but uses a *WMAP*7 cosmology.[2] The simulation uses 2160^3 particles in a $(500\,h^{-1}\,\mathrm{Mpc})^3$ box, corresponding to a particle mass of $9.31 \times 10^8\,h^{-1}\,\mathrm{M}_\odot$. There are 61 simulation outputs between $z = 50$ and 0.

Halo merger trees are constructed from the simulation outputs. These trees are the starting point for the SAMs. Both the G13 and GP14 use a friends-of-friends (FoF) group finding algorithm (Davis et al. 1985) to identify haloes in each snapshot of the simulation, retaining those with at least 20 particles. SUBFIND is then run on these groups to identify subhaloes (Springel et al. 2001). The merger trees differ from this point on. G13 construct dark matter halo merger trees by linking a subhalo in one snapshot to a single descendant subhalo in the subsequent output. The halo merger tree used in L-GALAXIES is therefore a subhalo merger tree. GP14 use the `Dhalo` merger tree construction (Merson et al. 2013; Jiang et al. 2014) that also uses the outputs of the `FoF` and SUBFIND algorithms. The `Dhalo` algorithm applies conditions on the amount of mass stripped from a subhalo and its distance from the centre of the main halo before it is considered to be merged with the main subhalo. Also, subsequent output times are examined to see if the subhalo moves away from the main subhalo, to avoid merging subhaloes which have merely experienced a close encounter before moving apart. GALFORM post-processes the `Dhalo` trees to ensure that the halo mass increases monotonically with time.

The definition of halo mass used in the two models is not the same. The `Dhalo` mass used in GALFORM corresponds to an integer number of particle masses whereas a virial mass is calculated in L-GALAXIES. This leads to differences in the halo mass function between the models. To compare the HODs predicted by the models, we need a common definition of halo mass. Jiang et al. (2014) showed that the `Dhalo` masses and virial halo masses can be related by applying a small offset in mass and a scatter. For simplicity, we chose instead to relabel the halo masses in GP14 by matching the abundance of dark matter haloes between models and using the mass from G13.

[1] The G13 and GP14 outputs are publicly available from the Millennium Archive in Durham http://virgodb.dur.ac.uk/ and Garching http://gavo.mpa-garching.mpg.de/Millennium/.

[2] The values of the cosmological parameters used in the MS7 are: $\Omega_{\mathrm{m0}} = \Omega_{\mathrm{dm0}} + \Omega_{\mathrm{b0}} = 0.272$, $\Omega_{\Lambda 0} = 0.728$, $\Omega_{\mathrm{b0}} = 0.0455$, $\sigma_8 = 0.81$, $n_{\mathrm{s}} = 0.967$, $h = 0.704$.

2.2 The HOD

2.2.1 *HOD modelling*

The HOD formalism characterizes the relationship between galaxies and haloes in terms of the probability distribution that a halo of virial mass M_{h} contains N galaxies of a given type, together with the spatial and velocity distributions of galaxies inside haloes. The key ingredient is the halo occupation function, $\langle N(M_{\mathrm{h}})\rangle$, which represents the average number of galaxies as a function of halo mass. The advantage of this approach is that it does not rely on assumptions about the (poorly understood) physical processes that drive galaxy formation and can be empirically derived from the observations.

Standard applications typically assume a cosmology as well as a parametrized form for the halo occupation functions motivated by the predictions of SAMs and hydrodynamics simulations (e.g. Zheng et al. 2005). The HOD parameters are then constrained using measurements of galaxy clustering measurements from large surveys and the theoretically predicted halo clustering. This approach essentially transforms measures of galaxy clustering into a physical relation between galaxies and dark matter haloes, setting the stage for detailed tests of galaxy formation models.

An important application of HOD modelling is to facilitate the generation of mock galaxy catalogues by populating dark matter haloes from an *N*-body simulation with galaxies that reproduce the desired clustering properties. This method has become popular due to its low computational cost and good performance (e.g. Manera et al. 2015; Zheng & Guo 2016; Smith et al. in preparation). Typically, the halo occupation function is available for an observational sample at a particular redshift, or over a narrow redshift interval. In order to generate a mock galaxy catalogue over a wide baseline in redshift using this technique, it is necessary to specify the HOD as a function of redshift or to have a prescription for its redshift evolution. SAMs predict the galaxy content of haloes and so the HOD is an output of these models. Here, we use the HOD to describe the model predictions at different redshifts for galaxy samples with different abundances.

2.2.2 *HOD parametrization*

For the parametrization of the HOD, it is useful to make a distinction between central galaxies, namely the main galaxy inside a halo, and the additional satellite galaxies that populate the halo, and consider separately the contributions of each (Kravtsov et al. 2004; Zheng et al. 2005). By definition, a dark matter halo cannot be populated by more than one central galaxy but, in principle, there is no limit to the number of satellite galaxies. Also, for samples defined by properties that scale with the halo mass, such as luminosity, a halo should be first populated by a central galaxy and then by a satellite galaxy. (One counterexample to this is when a selection involving colour is applied, as is the case with luminous red galaxies.) In SAMs, there is no unique way to define which is the central galaxy. Following a halo merger, L-GALAXIES defines a central galaxy as the most massive galaxy inside a halo in terms of the stellar mass. In GALFORM, the central galaxy is assumed to be the one from the

most massive progenitor halo. Despite this distinction, both models usually agree in their identification of the central.

The traditional shape assumed for the HOD is a rapid transition from zero to one galaxy for centrals and a transition from zero galaxies to a power law for satellite galaxies. One of the most commonly used parametrizations is the five-parameter model introduced by Zheng et al. (2005) (see also Zheng et al. 2007; Zehavi et al. 2011), which describes well samples of galaxies brighter than a given luminosity or more massive than a given stellar mass. Here, we will adopt this form of the halo occupation function to describe the predictions of the SAMS.

The mean occupation function of the central galaxies is a step-like function with a cutoff profile softened to account for the scatter between galaxy luminosity and halo mass. It has the following form:

$$\langle N_{\rm cen}(M_{\rm h})\rangle = \frac{1}{2}\left[1 + {\rm erf}\left(\frac{\log M_{\rm h} - \log M_{\rm min}}{\sigma_{\log M}}\right)\right], \quad (1)$$

where $M_{\rm h}$ is the host halo mass and erf(x) is the error function,

$${\rm erf}(x) = \frac{2}{\sqrt{\pi}}\int_0^x e^{-t^2}{\rm d}t. \quad (2)$$

$M_{\rm min}$ characterizes the minimum halo mass for hosting a central galaxy above the specified threshold. Its exact definition can vary between different HOD parametrizations. In the form we adopt here, it is the halo mass for which half of the haloes host a central galaxy above a given threshold (i.e. $\langle N_{\rm cen}(M_{\rm min})\rangle = 0.5$). The other parameter, $\sigma_{\log M}$, characterizes the width of the transition from zero to one galaxy per halo. A value of $\sigma_{\log M} = 0$ corresponds to a vertical step-function transition, while a non-zero value of $\sigma_{\log M}$ is indicative of the amount of scatter between stellar mass and halo mass. For samples defined by a luminosity threshold, it was further shown that $M_{\rm min}$ is the mass of haloes in which the mean luminosity of central galaxies is the luminosity threshold, and $\sigma_{\log M}$ is directly related to the width of the distribution of central galaxy luminosities (Zheng et al. 2005, 2007).

For satellite galaxies, the HOD is modelled as

$$\langle N_{\rm sat}(M_{\rm h})\rangle = \left(\frac{M_{\rm h} - M_{\rm cut}}{M_1^*}\right)^{\alpha}, \quad (3)$$

for $M_{\rm h} > M_{\rm cut}$, representing a power-law occupation function modified by a smooth cutoff at small halo masses. Here, α is the slope of the power law, which typically has a value close to unity, $M_{\rm cut}$ is the satellite cutoff mass scale (i.e. the minimum mass of haloes hosting satellites) and M_1^* is the normalization of the power law. A useful parameter that is often discussed is M_1, the mass of haloes that on average have one satellite galaxy, defined by $\langle N_{\rm sat}(M_1)\rangle = 1$. Note that M_1 is different from M_1^* above, but is obviously related to the values of M_1^* and $M_{\rm cut}$ ($M_1 = M_{\rm cut} + M_1^*$).

The occupation functions for centrals and satellites can be fitted independently with this definition, with the total number of galaxies given by their sum:

$$\langle N_{\rm gal}(M_{\rm h})\rangle = \langle N_{\rm cen}(M_{\rm h})\rangle + \langle N_{\rm sat}(M_{\rm h})\rangle. \quad (4)$$

A schematic representation of the shape of the HOD illustrating which features are sensitive to the various parameters is shown in Fig. 1.

Other works have also applied the cutoff profile used for the central galaxies occupation function to the satellites, effectively assuming (using our notation) that the total number of galaxies is given by $\langle N_{\rm cen}\rangle(1 + \langle N_{\rm sat}\rangle)$ (e.g. Zheng et al. 2007, 2009; Zehavi et al. 2011; Guo et al. 2015b). In this case, the fitting of the HOD

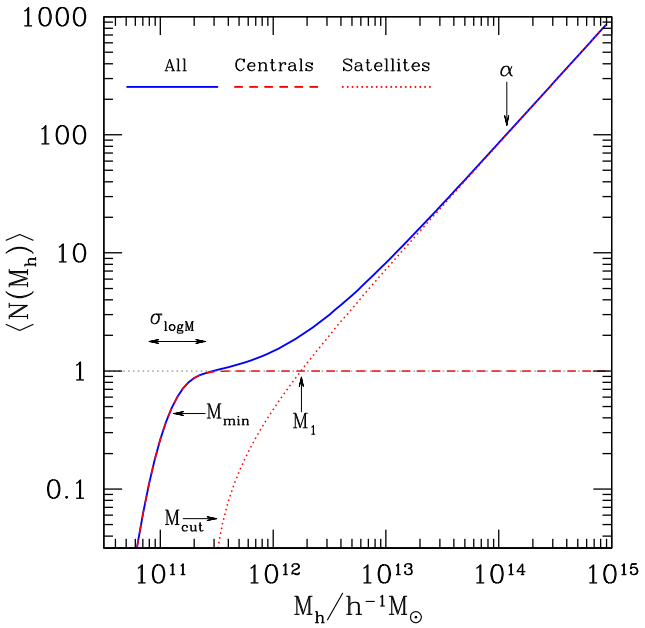

Figure 1. A schematic depicting the standard five-parameter form of the HOD, which gives the mean number of galaxies per halo as a function of host halo mass. The solid blue line shows the occupation function for all galaxies, which can be broken up into the contribution from central galaxies (red-dashed line) and satellite galaxies (red-dotted line). To guide the eye, a grey dotted line is plotted at $\langle N(M_{\rm h})\rangle = 1$; this will be shown in all subsequent HOD plots. The halo occupation function of central galaxies shows a gradual transition from zero to one galaxy per halo and can be well described by two parameters; $\sigma_{\log M}$, which describes the smoothness of this transition, and $M_{\rm min}$, which is the halo mass at which half of the haloes are populated by a central galaxy. The satellites occupation function is described as a transition from zero galaxies to a power law and is characterized by three parameters: $M_{\rm cut}$ the minimum halo mass at which satellites first populate dark matter haloes; M_1 the mass where there is an average of one satellite galaxy per halo; and α, the power-law slope. For a full description of these parameters, see Section 2.2.2.

cannot be done separately for centrals and satellites (because of the $\langle N_{\rm cen}\rangle\langle N_{\rm sat}\rangle$ term). Hence, assuming this form results in a more complex procedure to determine the best-fitting values of the parameters and ultimately gives poorer constraints, particularly for $M_{\rm cut}$. This assumption is often used when the HOD is inferred from the measured projected correlation function. Caution must be taken before comparing results obtained with this formalism and the one presented here.

When inferring the HOD from measured galaxy clustering, one needs to specify the mean value of $\langle N_{\rm cen}N_{\rm sat}\rangle$ at each halo mass when computing the one-halo central–satellite pairs. It is often implicitly assumed that a halo hosting a satellite galaxy also hosts a central galaxy from the same sample. Alternatively, one can assume independent central and satellite occupations and approximate this term as $\langle N_{\rm cen}\rangle\langle N_{\rm sat}\rangle$ (see discussion in Zheng et al. 2005; Guo et al. 2014, 2015a). The exact level of the correlation between central and satellite galaxies is determined by galaxy formation physics. While not relevant to our direct computations of the HOD in the SAMs in this paper, we can use the output of the SAMs to assess the impact of the central–satellite correlation and test the assumption that $\langle N_{\rm cen}N_{\rm sat}\rangle \simeq \langle N_{\rm cen}\rangle\langle N_{\rm sat}\rangle$. Fig. 2 shows these two quantities plotted as a function of halo mass for samples with different galaxy number densities using the output of the G13 SAM. We find only negligible difference between these two terms for small occupation

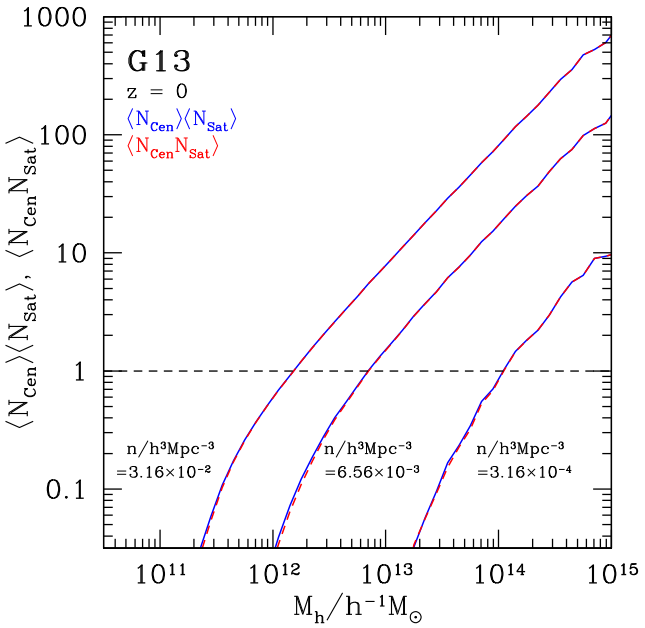

Figure 2. A test of the assumption, often made in HOD modelling, that $\langle N_{\rm sat}\rangle\langle N_{\rm cen}\rangle$ (blue lines) and $\langle N_{\rm sat}N_{\rm cen}\rangle$ (red lines) are equivalent. These quantities are shown as a function of halo mass in the G13 model for three number densities: $n = 3.16 \times 10^{-2}\,h^3\,{\rm Mpc}^{-3}$, $n = 6.56 \times 10^{-3}\,h^3\,{\rm Mpc}^{-3}$ and $n = 3.16 \times 10^{-4}\,h^3\,{\rm Mpc}^{-3}$ (moving from left to right in order of decreasing density) at $z = 0$. These two quantities are indeed equivalent in the SAM output.

values, demonstrating that this approximation is indeed valid for these number densities.

3 THE EVOLUTION OF THE HOD

This section contains our main results. In Section 3.1, we introduce the galaxy samples studied and plot the HODs predicted for these samples by the SAMs. In Section 3.2, we show how the HODs evolve with redshift. Fits to the HODs are given in Section 3.3. In Section 3.4, we quantify the evolution of the best-fitting parameters. Finally, in Section 3.5, we show the evolution of the ratio between M_1 and $M_{\rm min}$, two of the HOD parameters often used to characterize the galaxy–halo relation.

3.1 HOD for galaxy samples with different number densities

For the main part of our work, we use the number density of galaxies ranked in order of decreasing stellar mass to define our galaxy samples in the SAM catalogues. We build galaxy samples for a wide range of number densities: $n = 3.16 \times 10^{-2}$, 1×10^{-2}, 6.56×10^{-3}, 3.16×10^{-3}, 1×10^{-3} and $3.16 \times 10^{-4}\,h^3\,{\rm Mpc}^{-3}$ and redshifts: $z = 0$, 0.5, 1.1, 1.5, 2, 2.6 and 3. The cumulative comoving number density of galaxies as a function of stellar mass is commonly used to try to link galaxy populations across cosmic time (Leja et al. 2013; Mundy, Conselice & Ownsworth 2015; Torrey et al. 2015, see also our discussion in Section 4). It is inspired by the same hypothesis that motivates the passive evolution model (Section 4), is better defined than a constant stellar mass selected sample, being insensitive to systematic shifts in the stellar mass calculation, and is readily reproducible in observations. Contreras et al. (2013) have also shown that HOD predictions for such samples are quite robust among different SAMs at a fixed redshift. While the samples in this work are all ranked by stellar mass, our main results regarding the HOD evolution also hold when defining galaxy samples using other galaxy properties that scale with the halo mass, e.g. luminosity.

The samples were chosen to be evenly spaced in logarithmic number density, with each one corresponding to a change of half a decade in log abundance. There are three densities in particular which we use to illustrate our main results: (i) $3.16 \times 10^{-2}\,h^3\,{\rm Mpc}^{-3}$, which is close to the number density studied by Zheng et al. (2005) in their comparison between SAMs and hydrodynamical simulations, (ii) $6.56 \times 10^{-3}\,h^3\,{\rm Mpc}^{-3}$, which is roughly the number density of galaxies brighter than L^* in the SDSS Main Sample (Zehavi et al. 2011) and (iii) $3.16 \times 10^{-4}\,h^3\,{\rm Mpc}^{-3}$, which is comparable to the number density of luminous red galaxies in the SDSS-III Baryonic Oscillation Spectroscopic Survey (Eisenstein et al. 2011).

Fig. 3 shows the cumulative stellar mass function for all redshifts studied. The horizontal dashed lines show the different number density cuts we consider. The galaxies selected for a given number density are those to the right of the intersection with their associated dashed line. For ease of reference, we specify the corresponding stellar mass thresholds at $z = 0$ later on in Tables 1 and 2.

Fig. 4 shows the correlation functions and halo occupation functions calculated directly in the GP14 SAM, for all number densities at $z = 0$. The clustering amplitude correlation increases monotonically as the galaxy number density decreases (corresponding to more massive, or more luminous, galaxies). The HOD shifts towards higher halo masses as the galaxy number density decreases, which means that more massive galaxies occupy more massive haloes. Also, with decreasing number density, the transition between zero and one central galaxy per halo becomes broader which makes the plateau in the halo occupation where it is dominated by central galaxies less pronounced. Similar results are found for G13, and the implications for the HOD parameters (for both) are shown and discussed in Section 3.3. Identical trends were found by Zehavi et al. (2011) using the SDSS for samples of varying luminosity thresholds.

3.2 The evolution of the HOD with redshift

There are several reasons why the evolution of the HOD is interesting: (1) it allows us to characterize galaxy evolution, (2) if we can parametrize the evolution, the HOD can be used to build mock galaxy catalogues that cover a broad range of number densities and redshifts and (3) observed clustering measures at different epochs can be modelled consistently.

The choice of using the halo occupation function to quantify the evolution in the galaxy population has some distinct advantages over utilizing the correlation function. The halo occupation function itself does not depend on the distribution of galaxies within a halo, which is something different galaxy formation models have modelled in different ways to date (see, for example the discussion in Contreras et al. 2013). Furthermore, the HOD is a function of halo mass, which makes it easier to interpret in terms of the implications for galaxy formation models. Finally, the parameters of the HOD give fundamental information about the galaxy sample (as shown in Sections 3.4 and 3.5). The predictions for the redshift evolution of the HOD have not been widely studied over a large redshift range, and such an investigation can inform empirical treatments of the evolution (e.g. Coupon et al. 2012; de la Torre et al. 2013; Skibba et al. 2015).

The redshift evolution of the HODs and the correlation functions predicted by the G13 and GP14 models are shown in Fig. 5 for

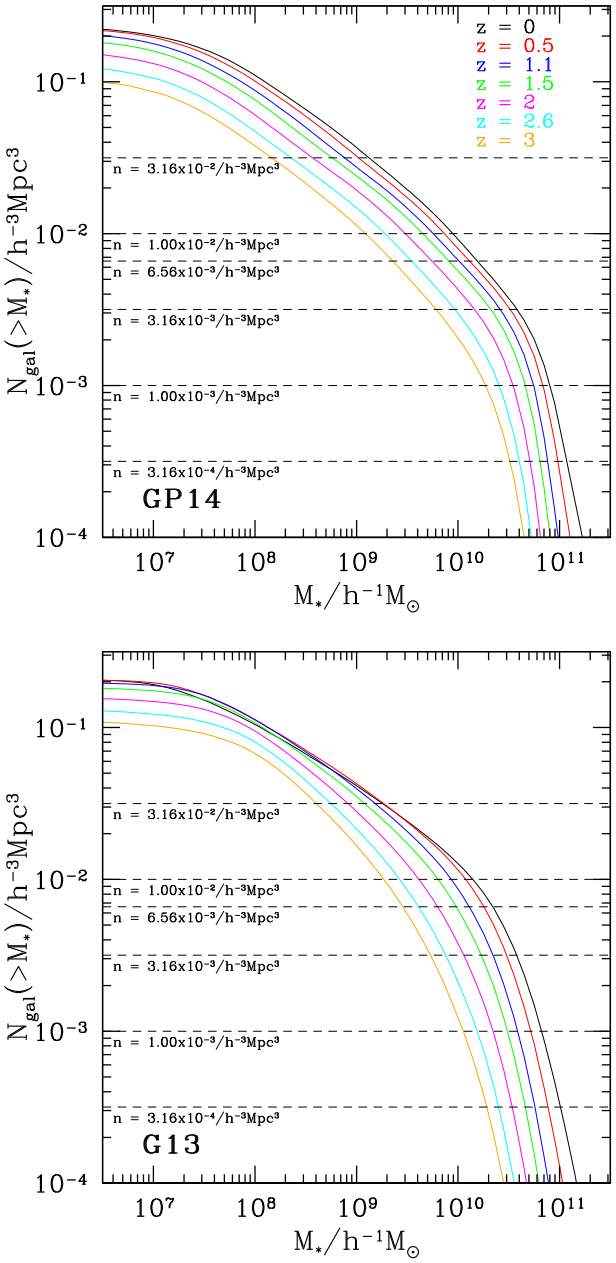

Figure 3. The cumulative stellar mass function in the GP14 (top) and G13 (bottom) models. The different lines represent different redshifts as labelled in the top panel, with the redshift increasing from top to bottom. The dashed horizontal lines show the number density cuts adopted, which are labelled by the value of the number density. The galaxies selected for a given number density are those to the right of the intersection with their associated dashed line.

galaxy samples with a number density of $6.56 \times 10^{-3}\,h^{-3}$ Mpc. The clustering amplitude increases with time, corresponding to the mean occupation functions shifting towards larger masses with decreasing redshift. This trend is mostly due to the process of hierarchical accretion, i.e. the evolution of the halo mass function, coupled with the evolution of galaxy bias. In fact, the halo mass function exhibits stronger evolution and dominates this trend. We also examined the HOD evolution when plotting the occupation functions against

Table 1. The values of M_1, $M_{\rm min}$, $M_{\rm cut}$, α and $\sigma_{\log M}$ for the GP14 model at $z = 0$, shown for the six fixed number density samples. We also provide the corresponding stellar mass thresholds, $M_*^{\rm thres}$, for these samples. All masses are in units of $h^{-1}{\rm M}_\odot$.

$n/h^{-3}{\rm Mpc}^3$	$\log M_*^{\rm thres}$	$\log M_1$	$\log M_{\rm min}$	$\log M_{\rm cut}$	α	$\sigma_{\log M}$
3.16×10^{-4}	11.02	14.17	13.43	12.79	1.09	0.86
1.00×10^{-3}	10.86	13.66	13.06	12.36	1.05	1.03
3.16×10^{-3}	10.53	13.16	12.46	12.11	1.09	0.93
6.56×10^{-3}	10.14	12.88	12.02	11.84	1.11	0.86
1.00×10^{-2}	9.90	12.71	11.74	11.75	1.09	0.76
3.16×10^{-2}	9.07	12.25	11.11	11.42	1.06	0.24

Table 2. Same as Table 1 (parameter values at $z = 0$), but for the G13 model.

$n/h^{-3}{\rm Mpc}^3$	$\log M_*^{\rm thres}$	$\log M_1$	$\log M_{\rm min}$	$\log M_{\rm cut}$	α	$\sigma_{\log M}$
3.16×10^{-4}	10.96	14.04	13.36	12.81	1.12	0.66
1.00×10^{-3}	10.77	13.61	12.92	12.41	1.06	0.87
3.16×10^{-3}	10.53	13.15	12.28	12.08	1.03	0.73
6.56×10^{-3}	10.29	12.84	11.83	11.90	1.01	0.61
1.00×10^{-2}	10.10	12.66	11.62	11.74	1.01	0.21
3.16×10^{-2}	9.21	12.19	11.12	11.26	1.02	0.13

$M_{\rm h}/M_{\rm C}^*$, where $M_{\rm C}^*$ is the characteristic mass[3] of the halo mass function. We find much weaker evolution of the mass parameters which determine the form of the HOD than is experienced by the characteristic mass of the halo mass function over the same redshift interval.

The overall evolution of the HOD is similar in the two models. The evolution of the correlation function shows subtle differences between the models, particularly on small scales dominated by the distribution of satellite galaxies. These differences likely arise due to the different treatment of satellites in the models (Section 2.1.1), specifically with regard to the distribution and evolution of satellites that have lost their subhalo. These galaxies (known as orphan galaxies) are located in the inner part of the halo and contribute to the correlation function on small scales (Contreras et al. 2013). We have examined them in detail for the $n = 6.56 \times 10^{-3}\,h^3\,{\rm Mpc}^{-3}$ case, and find that in G13 there is a roughly constant fraction of orphan satellite galaxies with redshift. The fraction is smaller than that in GP14, which explains why the correlation function is similar for all redshifts on small scales in G13 and is lower in amplitude than GP14.

The qualitative trends are also similar for the other samples with different number densities. The amount of information we can obtain from visual inspection, however, is limited. To make a more quantitative study, we proceed to fit the five-parameter form to the HODs predicted by the models for the different samples and compare the best-fitting values.

3.3 Fitting the HOD predicted by SAMs

To quantify the evolution of the HOD, we study the change of the best-fitting parameters as a function of redshift and number density. The HOD parametrization we use is the five-parameter one

[3] The characteristic halo mass, $M_{\rm C}$, is defined by $\delta_{\rm C} = \sigma(M_{\rm C}, z)$, where $\delta_{\rm C}$ is the linear theory threshold for collapse at redshift z and $\sigma(M)$ is the linear theory variance on a scale that contains uncollapsed mass M (Rodríguez-Puebla et al. 2016).

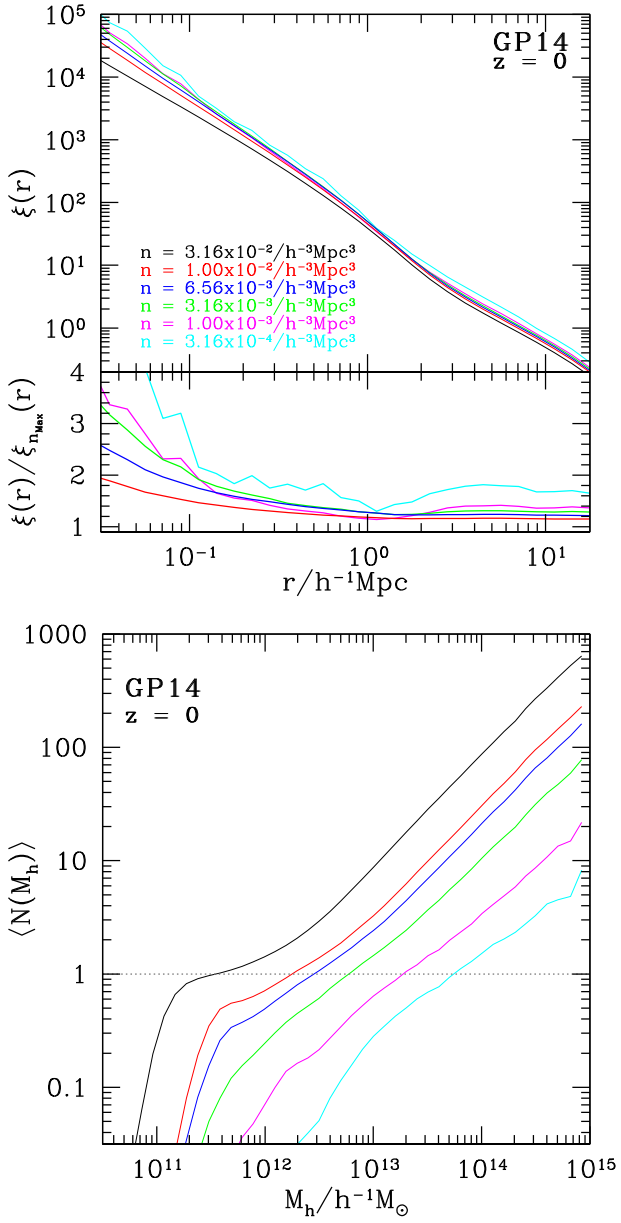

Figure 4. The correlation function (top panel) and HOD (bottom panel) at $z = 0$ for the GP14 model. The different colours represent different number densities as labelled on the top panel. In the bottom part of the top panel, we show the ratio between the correlation functions for different number densities and the one corresponding to the highest number density ($n = 3.16 \times 10^{-2}\,h^3\mathrm{Mpc}^{-3}$). In the top panel, the number density increases from top to bottom. In the bottom panel, the number density decreases from top to bottom.

presented in Section 2.2.2. To make a more accurate fit of the model HOD, we consider the central and satellite galaxies separately, using the classification assigned by the models. The fits are carried out using a χ^2 minimization method expressed in terms of the logarithm of the number density of galaxies. We only consider haloes for which the mean occupation satisfies $\langle N(M_\mathrm{h})\rangle > 0.1$. This limit was adopted because it is lower than the amplitude of the HOD that is typically constrained in observational studies. Also, in this range we are not affected by issues which arise from the construction of the merger tree used by the SAMs (Contreras et al. 2013). Furthermore, the shape of the HOD in this regime is better described by the five-parameter form adopted.

When fitting the HOD, we weight all mass bins equally. We tested weighting the mass bins by the number of haloes they contain and by their contribution to the effective bias. However, applying weights in these ways tends to overemphasize a particular part of the HOD leading to considerable discrepancies at high halo masses. Instead, we treat each mass bin as having the same error. As is standard practice in such cases, the uncertainty on the best-fitting parameters is determined from the χ^2 values once normalized to $\chi^2_\mathrm{min}/\mathrm{d.o.f.} = 1$.

Figs 6 and 7 show the occupation functions determined from the SAMs together with their best-fitting five-parameter models for GP14 and G13, respectively. The halo occupation functions are shown for three representative number densities and for $z = 0$ and 1. The fitted HODs generally produce good fits for all cases over most of the range. A deviation is seen in a couple of the cases at the very low mass end, related to fitting only above $\langle N(M_\mathrm{h})\rangle > 0.1$ (however lowering this limit in an attempt to remedy these discrepancies generally resulted in a worse fit in the turnover of the central occupation function).

The predicted occupation functions look very similar in the two models for the sample with the highest number density of galaxies (top panels). There is a clear plateau in the total halo occupation due to central galaxies until the halo mass at which the satellites power law starts to dominate. For the intermediate number density sample, in the GP14 model the central HOD reaches unity around the same mass that the satellite occupation does. In contrast, for the G13 model the central occupation reaches unity at a lower halo mass than the satellite occupation, which results in more of a step-like shape for the overall HOD. This reflects differences in the treatment of the suppression of cooling by active galactic nuclei in the two models. For the lowest number density sample, both models display a very broad turnover in the central occupations and no distinct plateau. The central galaxy HOD does reach unity for this sample (though only just for the GP14 model at $z = 1$).

Some subtle general differences with redshift are noticeable for all number density samples and both models. Going towards higher redshift, the plateau in the mean halo occupation decreases somewhat and the width of the central occupation appears to change. We examine the evolutionary changes in detail in Section 3.4.

3.4 Modelling the HOD evolution

To quantify the evolution of the HOD, we focus on how the best-fitting parameters change with redshift. Fig. 8 shows the values of the best-fitting parameters for the full range of redshifts and number densities studied (solid lines connecting points with error bars).

Fig. 8 allows us to assess which evolutionary behaviour in the HOD parameters is generic and independent of the modelling choices and assumptions. The halo mass for which there is typically one satellite galaxy per halo, M_1, evolves in a remarkably similar way in both models, declining by 0.6 dex between $z = 0$ and 3. This is much weaker than the evolution expected in the characteristic halo mass which changes by four orders of magnitude over the same redshift interval (Rodríguez-Puebla et al. 2016). The evolution of M_min, the minimum halo mass at which half the haloes host a central galaxy evolves in a similar way between the models for the four highest density galaxy samples. For the two samples with the lowest space densities of galaxies, M_min increases with redshift in the GP14 model, but continues to decline with increasing redshift in G13. Globally (with the exception of the two least

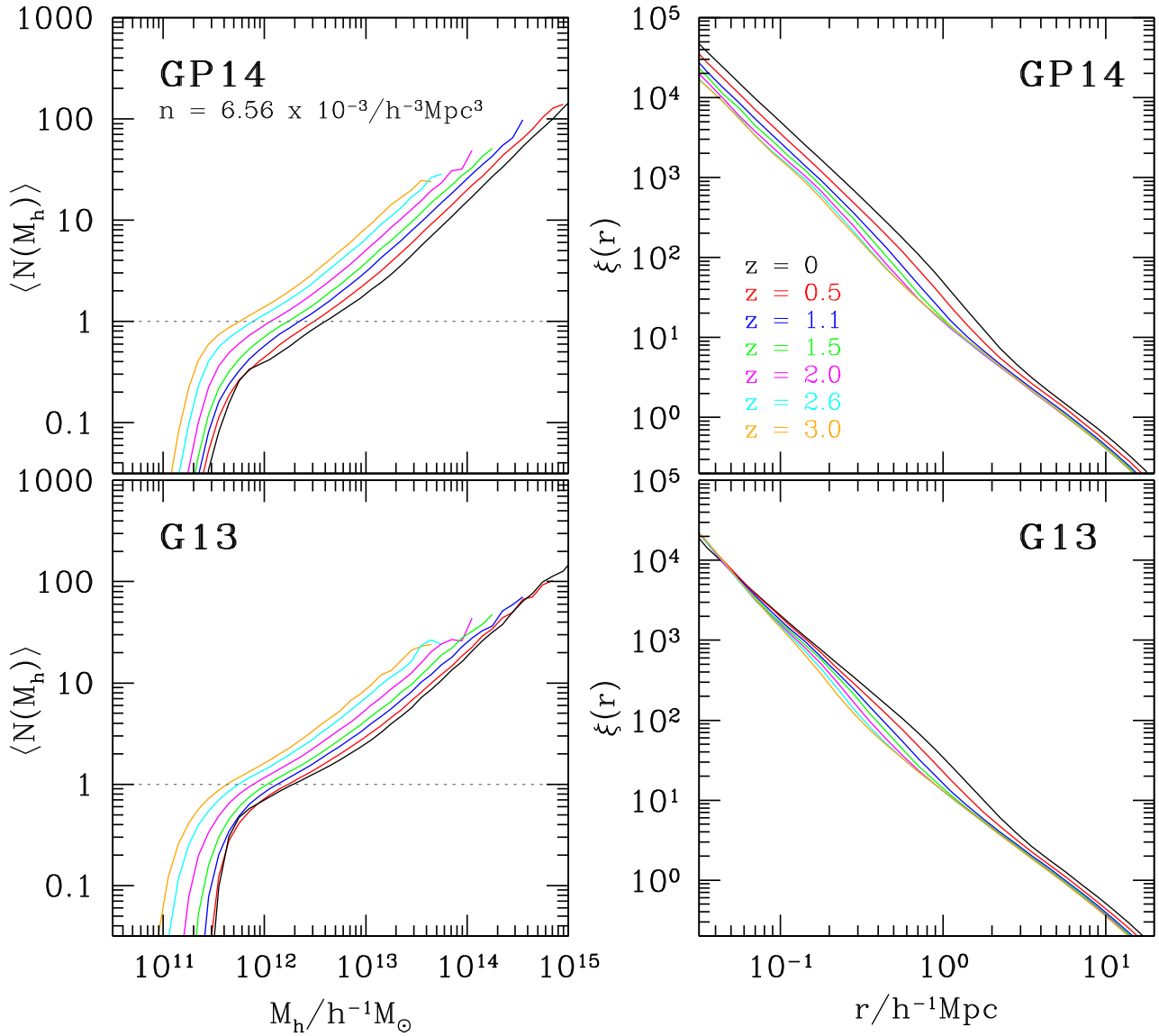

Figure 5. The evolution with redshift of the HOD (left-hand panel) and correlation function (right-hand panel) for a galaxy sample with number density $n = 6.56 \times 10^{-3}\,h^3\,\mathrm{Mpc}^{-3}$. The top panels show the predictions of the GP14 model and the bottom panels show the predictions for the G13 model. The different colours indicate different redshifts as labelled in the top-right panel. In the left-hand panel, the redshift decreases from top to bottom. In the right-hand panel, the redshift increases from top to bottom.

abundant samples in GP14), the evolution seems more modest for $M_{\rm min}$ than we found for M_1: $M_{\rm min}$ is roughly constant to $z \sim 0.75$ before dropping by 0.2–0.6 dex depending on the abundance of the sample. $M_{\rm cut}$, the cutoff mass for hosting a satellite galaxy, evolves in a similar way in G13 and GP14, though the results for the least abundant sample in GP14 have large errors. The slope of the satellite HOD power laws is different between the models but shows little dependence on redshift. The largest differences are found in the evolution of the width of the transition from zero to unity in the central galaxy HOD. We have checked the evolution of the parameters also with earlier SAM catalogues from the two groups and generally find a similar behaviour to that shown by the models studied here.

To quantify the evolution of the best-fitting HOD parameters, we use a single evolutionary parameter for each property, γ, along with the value of the parameter at $z = 0$. This approach will allow us to specify the value of the parameter at redshifts intermediate to the ones where we have SAM outputs, which will be important for building mock catalogues, as well as provide a generalized form of the HOD as a function of redshift. We fit these for each of our number density samples independently using the values of the fitting parameters shown in Fig. 8. We represent the value of M_1 as a function of redshift as a power law:

$$\log M_1(z) = \log M_1(z=0) + \gamma_{M_1} \times z. \quad (5)$$

For $M_{\rm min}$ and $M_{\rm cut}$, we use a constant value from $z = 0$ to 0.75, followed by a power law;

$$\log M_{\rm min}(z) = \begin{cases} \log M_{\rm min}(z=0) & \text{if } z \le 0.75 \\ \log M_{\rm min}(z=0) + (z-0.75) \times \gamma_{M_{\rm min}} & \text{if } z > 0.75, \end{cases} \quad (6)$$

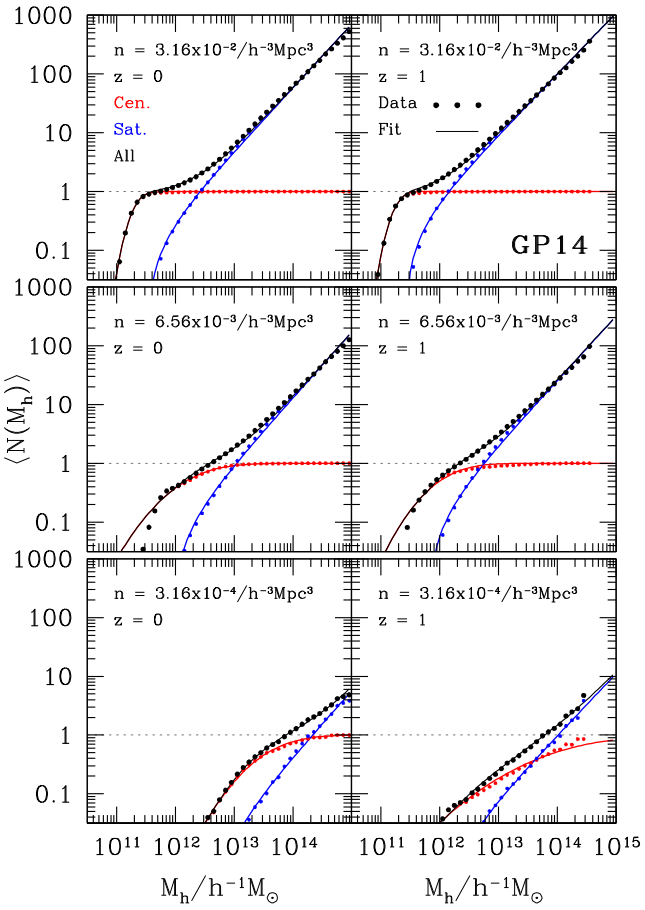

Figure 6. Measured and fitted halo occupation functions for the GP14 model at $z = 0$ (left-hand panels) and $z = 1$ (right-hand panels) for three representative number densities: $3.16 \times 10^{-2}\,h^3\,\mathrm{Mpc}^{-3}$ (top), $6.56 \times 10^{-3}\,h^3\,\mathrm{Mpc}^{-3}$ (middle) and $n = 3.16 \times 10^{-4}\,h^3\,\mathrm{Mpc}^{-3}$ (bottom). Dots show the HODs predicted by the SAMs and the lines show the five-parameter model best fits to them. Black dots and lines represent all galaxies, the central galaxies are shown in red and the satellites in blue.

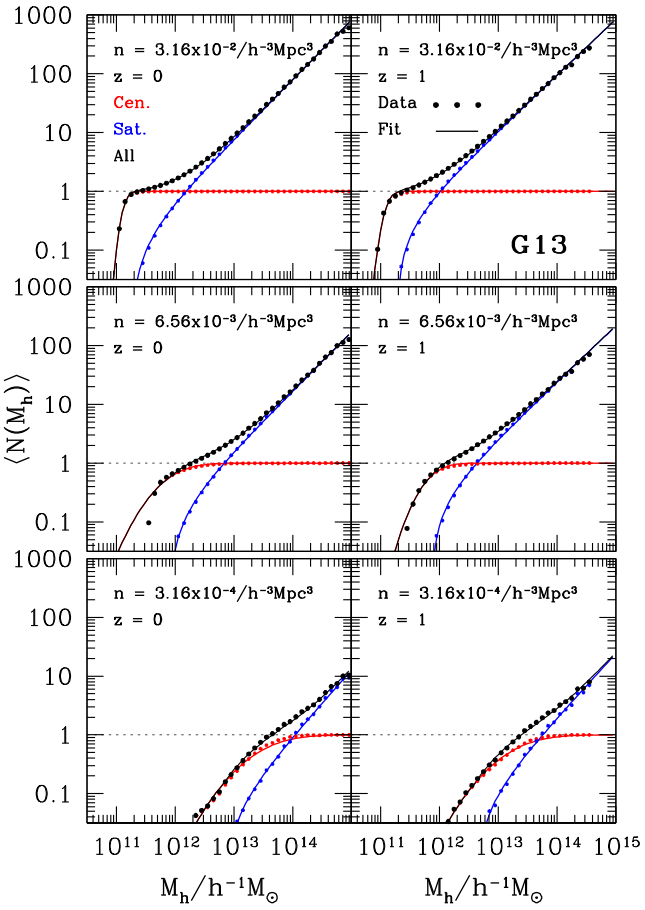

Figure 7. The same as in Fig. 6 but for the G13 model.

and

$$\log M_{\rm cut}(z) = \begin{cases} \log M_{\rm cut}(z=0)) & \text{if } z \le 0.75 \\ \log M_{\rm cut}(z=0) + (z-0.75) \times \gamma_{M_{\rm cut}} & \text{if } z > 0.75. \end{cases} \quad (7)$$

For α, we use a power-law value from $z = 0$ to 0.75, followed by a constant value;

$$\alpha(z) = \begin{cases} \alpha(z=0) + z \times \gamma_\alpha & \text{if } z \le 0.75 \\ \alpha(z=0) + 0.75 \times \gamma_\alpha & \text{if } z > 0.75. \end{cases} \quad (8)$$

Finally, for $\sigma_{\log M}$ we model the evolution as linear in redshift

$$\sigma_{\log M}(z) = \sigma_{\log M}(z=0) + \gamma_{\sigma_{\log M}} \times z. \quad (9)$$

Note that this is a first-order approximation, since we were not able to find a simple form that describes the evolution of this parameter.

The fits to the evolution of the HOD parameters are shown by the dotted lines in Fig. 8. The values of the parameters at $z = 0$ are presented in Tables 1 and 2, while the values for the evolutionary parameters (γ) are shown in Tables 3 and 4, for GP14 and G13, respectively.

We have also compared the evolution of the fitting parameters M_1 and $M_{\rm min}$ with their exact values extracted from the HOD (i.e. the halo mass of which $\langle N_{\rm sat}(M = M_1)\rangle = 1$ and $\langle N_{\rm cen}(M = M_{\rm min})\rangle = 0.5$). We find good agreement between these values and those obtained by fitting the HOD. Also, their redshift evolution is consistent with the models proposed in this work. We show that at least for these two parameters, the evolution is well constrained. Thus, we do not expect that any potential degeneracy in the fitting of the parameters would affect the evolutionary model we propose.

To test the accuracy of this approximation for the evolution of the HOD parameters, we plot in Fig. 9 the occupation functions obtained using the parameter values derived from our fits for the redshift dependence (equations 5– 9; labelled 'Evolved HOD' in the plot) and compare these with the occupation functions predicted by the SAM (labelled 'Actual HOD'). We do this for G13 at $z = 1$ and for three different number densities: $3.16 \times 10^{-4}\,h^3\,\mathrm{Mpc}^{-3}$ (cyan lines), $6.56 \times 10^{-3}\,h^3\,\mathrm{Mpc}^{-3}$ (blue lines) and $3.16 \times 10^{-2}\,h^3\,\mathrm{Mpc}^{-3}$ (black lines). We have used G13 for this exercise since the HODs predicted by this model are better described by the five-parameter fit over a wider range of number densities and redshifts than is the case for the GP14 model.

Fig. 9 shows that the halo occupations obtained from the parameter evolution fits are a reasonably good match to the direct output by the models at all number densities. The main differences are found at lower halo masses and are caused by the limitations in fitting $\sigma_{\log M}$. An alternative way of modelling the parameter evolution is shown by the dash–dotted lines (labelled 'Evolved HOD with fixed number density' in the plot). In this case, instead of fitting $\sigma_{\log M}$, we have set the other parameters to the values given by the evolutionary fit, and we fix the value of $\sigma_{\log M}$ to reproduce the number density

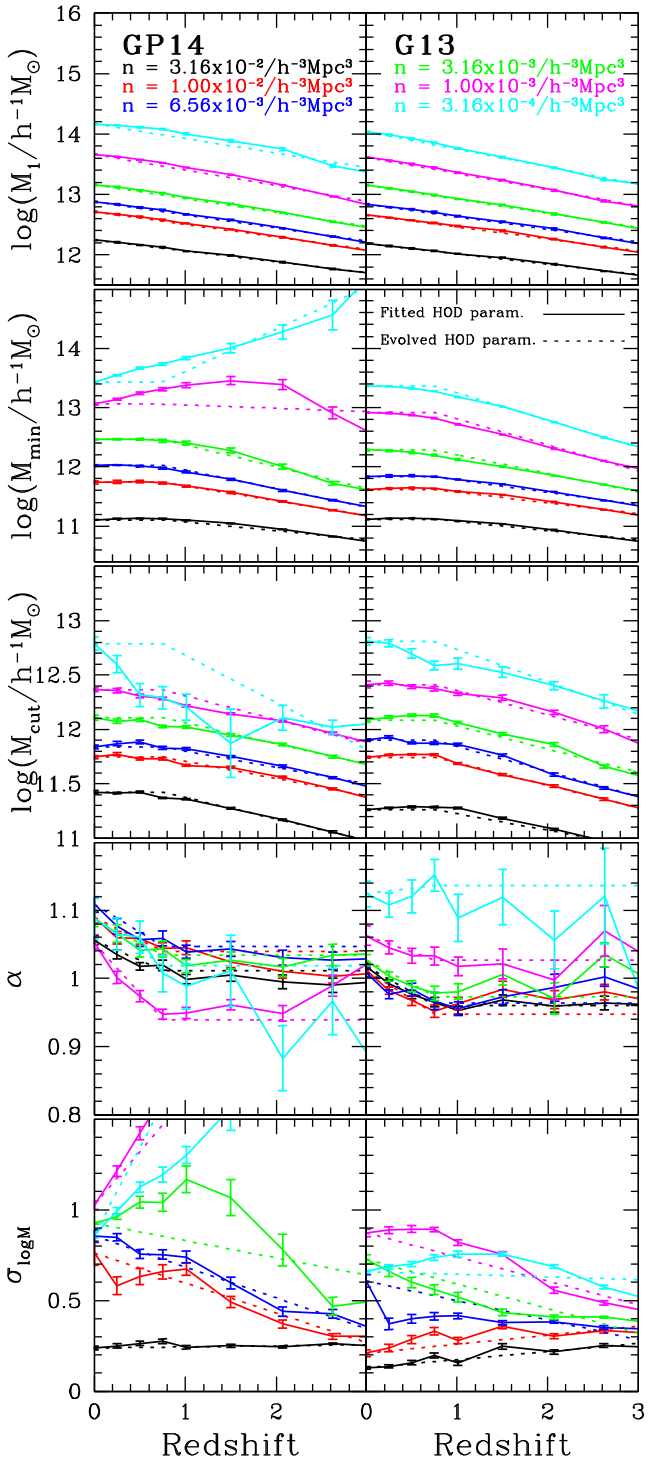

Figure 8. The evolution with redshift of the five HOD parameters, after fitting to the predictions of the GP14 (left) and G13 (right) SAMs. From top to bottom, the properties shown in each row are: M_1, $M_{\rm min}$, $M_{\rm cut}$, α and $\sigma_{\log M}$. The different colours represent different number densities as labelled in the top panels. Error bars represent the standard deviation from the fitted parameter value (as explained in the text). Dotted lines represent the fits of equations (5)– (9). In the three top panels, the number density increases from top to bottom. In the two bottom panels, the number density tends to increase from top to bottom, except for the highest number densities (where the HOD is not well defined).

Table 3. The values of the evolution parameters γ for M_1, $M_{\rm min}$, $M_{\rm cut}$, α and $\sigma_{\log M}$ for the GP14 model, shown for the six fixed number density samples.

$n/h^{-3}{\rm Mpc}^3$	$\gamma_{\log M_1}$	$\gamma_{\log M_{\rm min}}$	$\gamma_{\log M_{\rm cut}}$	γ_α	$\gamma_{\sigma_{\log M}}$
3.16×10^{-4}	−0.24	0.49	−0.43	−0.09	0.96
1.00×10^{-3}	−0.26	−0.01	−0.22	−0.15	0.59
3.16×10^{-3}	−0.23	−0.24	−0.19	−0.07	−0.10
6.56×10^{-3}	−0.22	−0.21	−0.15	−0.08	−0.17
1.00×10^{-2}	−0.21	−0.17	−0.16	−0.07	−0.16
3.16×10^{-2}	−0.18	−0.10	−0.20	−0.06	0.01

Table 4. Same as Table 3 (values of evolution parameters), but for the G13 model.

$n/h^{-3}{\rm Mpc}^3$	$\gamma_{\log M_1}$	$\gamma_{\log M_{\rm min}}$	$\gamma_{\log M_{\rm cut}}$	γ_α	$\gamma_{\sigma_{\log M}}$
3.16×10^{-4}	−0.29	−0.31	−0.30	0.02	−0.01
1.00×10^{-3}	−0.27	−0.30	−0.22	−0.05	−0.13
3.16×10^{-3}	−0.23	−0.21	−0.21	−0.07	−0.14
6.56×10^{-3}	−0.21	−0.14	−0.23	−0.06	−0.11
1.00×10^{-2}	−0.20	−0.12	−0.21	−0.09	0.05
3.16×10^{-2}	−0.17	−0.10	−0.15	−0.08	0.04

of the sample. The resulting HOD gives a better reproduction of the model HOD for the lower number density samples. At the highest number density, the values of the evolved parameters overestimate the number density. To compensate for this, $\sigma_{\log M}$ takes the minimum allowed value ($\sigma_{\log M} \sim 0$).

To investigate the significance of these deviations, we calculate the effective bias of the predicted G13 HODs at $z = 1$, following the procedure of Kim et al. (2009). We show the ratio of the different effective biases to that of the actual HOD in Fig. 9. The 'Evolved HOD' model shows small differences in the effective bias (<4 per cent) for the highest number density, while the lowest number density has a considerable difference of ∼25 per cent. In the case of 'Evolved HOD with fixed number density', we find differences $\lesssim$3 per cent for all number densities. This means that the first method can reliably reproduce the clustering signal at high number densities, while the second method can do so for a broader range of number densities. Interestingly, just fitting the HOD with the five-parameter model (labelled as 'Fitted HOD' in the figure) can by itself produce differences of over 10 per cent in the effective bias, due to the limitation of the accuracy with which this form can fit the detailed distribution.

We also test how the HOD evolves if α is kept constant. By evolving the HOD to $z = 1$, we find minimal differences in the HODs shown in Fig. 9. We thus note that the evolution of α has a minor impact on the evolution of the HOD at low redshifts.

Other approximations for the evolution of the HOD are mentioned in the literature. de la Torre et al. (2013) approximate jointly the HOD dependence on luminosity and redshift from VIPERS clustering measurements. Manera et al. (2015) incorporate a simplified evolving HOD to SDSS-III mock catalogues based on a compilation of HOD measurements (Parejko et al. 2013). Hearin et al. (2016) model the stellar-to-halo-mass relation based on abundance matching predictions (Behroozi, Conroy & Wechsler 2010). Direct comparison with these is not straightforward; however, due to differences in the sample definitions, HOD forms, approaches and assumptions made.

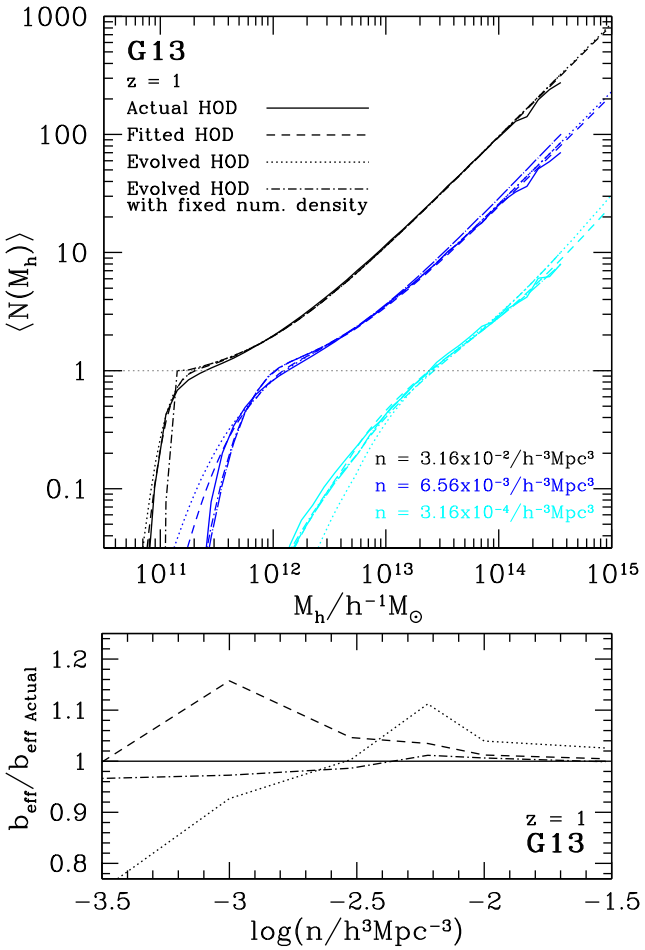

Figure 9. Top: the halo occupation functions for the G13 model at $z = 1$, for three number densities as labelled. The 'Actual HOD' results, i.e. the direct output in the simulation, are shown as solid lines. 'Fitted HOD' (dashed lines) corresponds to the five-parameter fits to the 'Actual HOD' at $z = 1$. The 'Evolved HOD' (dotted lines) is obtained from our fits to the redshift dependence of each parameter, evolved from their value at $z = 0$. Finally, 'Evolved HOD with fixed number density' (dot–dashed lines) shows the HOD assuming the redshift dependence for the fit parameters, but excluding $\sigma_{\log M}$, which instead is determined by requiring that the HOD fit reproduces the number density of the sample. The number density decreases from top to bottom. Bottom: effective bias ($b_{\rm eff}$) calculated for the 'Fitted HOD', 'Evolved HOD' and 'Evolved HOD with fixed number density' cases plotted relative to that of the 'Actual HOD' as function of number density, for the G13 model at $z = 1$. (See the text for more details.)

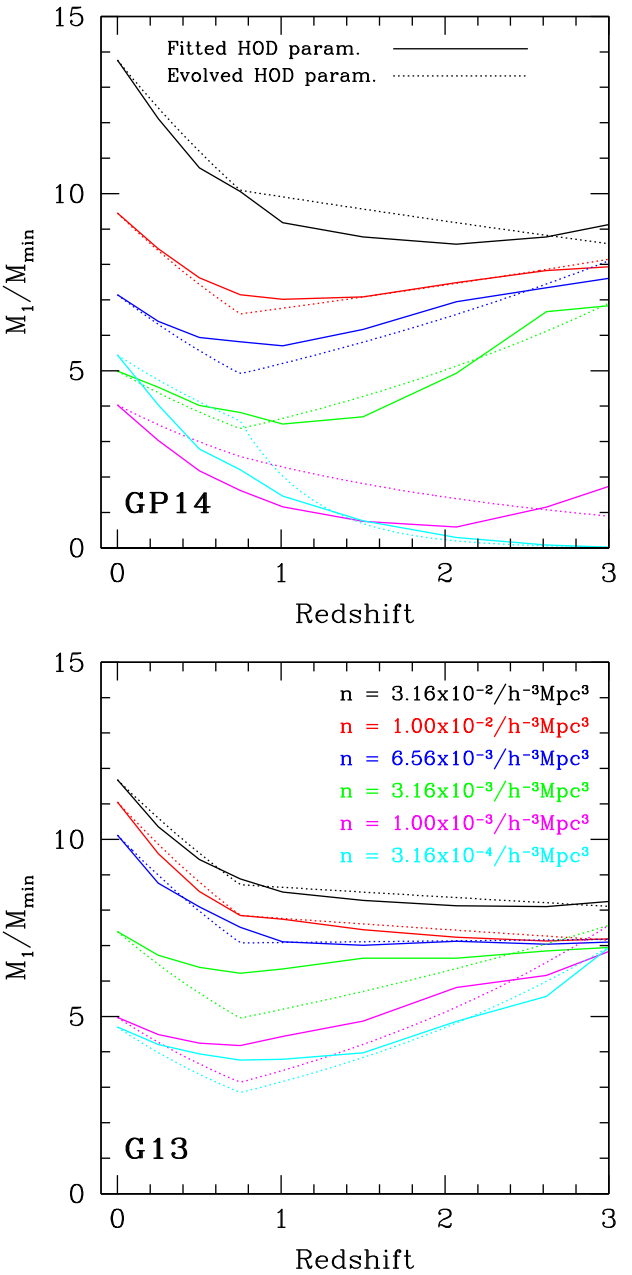

Figure 10. The ratio $M_1/M_{\rm min}$ plotted as a function of redshift for the GP14 (top) and G13 (bottom) panels. Different colours indicate different number densities as labelled. Solid lines show the ratio obtained from the best-fitting parameters to the HOD output by the models. Dashed lines show the ratio using the best-fitting redshift evolution using equations (5) and (6). The number density decreases from top to bottom (with the exception of the lowest number density sample, which crosses the adjacent sample for $z < 1.5$ in the top panel).

3.5 Evolution of the $M_1/M_{\rm min}$ ratio

One relation that is often extracted from the HOD is the ratio between the two characteristic halo masses, $M_1/M_{\rm min}$ (Zehavi et al. 2011; Coupon et al. 2012; Guo et al. 2014; Skibba et al. 2015). This ratio links the mass at which haloes start being populated by central galaxies (specifically, where $\langle N_{\rm cen}(M_{\rm min})\rangle = 0.5$) and the mass at which the halo starts hosting satellites as well (i.e. the halo mass for which $\langle N_{\rm sat}(M_1)\rangle = 1$). Larger values of $M_1/M_{\rm min}$ indicate that central galaxies populate haloes over a broader range of halo masses before satellite galaxies start to dominate, resulting in the 'plateau' feature in the HOD (as seen, for example in the high-density galaxy samples in Figs 6 and 7). Haloes in the 'hosting gap' mass range between $M_{\rm min}$ and M_1 tend to host more massive central galaxies rather than multiple galaxies (Berlind et al. 2003). The exact value of the ratio reflects the balance between accretion and destruction of the satellites (Zentner et al. 2005; Watson, Berlind & Zentner 2011) and the ratio also has a strong influence on the shape of the correlation function (e.g. Seo et al. 2008; Watson et al. 2011; Skibba et al. 2015).

Fig. 10 shows the evolution of $M_1/M_{\rm min}$ for the GP14 and G13 models, for our different number density samples. The solid line

shows the ratio between $M_1/M_{\rm min}$ obtained by fitting the HOD using equations (1) and (3), while the dotted line shows the prediction from the evolutionary model presented in the previous section (equations 5 and 6). The evolution of this ratio with redshift is complex. Its shape is different for each number density, and cannot be described by a simple functional form, though it is reassuring that our simple evolution model for $M_{\rm min}$ and M_1 also captures reasonably well the behaviour of their ratio.

We note that the value of $M_1/M_{\rm min}$ increases as we move to higher number densities (for any fixed redshift). This is in agreement with the results derived from observations (see e.g. fig. 4 of Guo et al. 2014). Decreasing the number density corresponds to more massive galaxies, which reside in more massive haloes, as we saw in Fig. 4. The trend we see likely reflects the relatively late formation of these massive haloes, which leaves less time for satellites to merge on to central galaxies and thus lowers the satellite threshold M_1 and this ratio.

As far as the redshift evolution, the ratio $M_1/M_{\rm min}$ decreases with redshift until $z \sim 0.75$ and then stays constant or increases (for all but the lowest number densities). The decrease for moderately increasing redshifts is probably due to a similar reasoning: for increasing redshift there is less time for destruction of the satellites resulting in a smaller ratio. For higher redshifts, $M_{\rm min}$ evolves as well and the trend halts or reverses and the exact behaviour is more complex to predict.

There are clear differences between the models we study in terms of the range of values of this ratio. This difference is perhaps related to the different treatment of satellites. Measurements of $M_1/M_{\rm min}$ and its evolution may thus provide strong constraints on models of galaxy formation.

Given the clear (yet complex) evolutionary trends present, we caution the reader against assuming an overall constant shift in halo mass of the halo occupation functions with redshift, corresponding to a constant ratio of $M_1/M_{\rm min}$. The broad sense of lower values for this ratio when going towards higher redshift is also consistent with predictions of abundance matching modelling in dissipationless simulations (Kravtsov et al. 2004; Conroy et al. 2006) as well as with inferred values from observations of galaxy clustering (e.g. Zheng et al. 2007; Coupon et al. 2012; Skibba et al. 2015).

4 COMPARISON WITH EMPIRICAL METHODS TO DESCRIBE THE EVOLVING GALAXY POPULATION

We now compare the evolution of the HOD predicted by SAMs with alternative heuristic approaches that are sometimes used in the literature to describe the evolution of the galaxy population. We focus on the evolution of the $M_1/M_{\rm min}$ ratio, which we already saw can provide important insight to galaxy formation and evolution, and on the change in the fraction of galaxies that are satellites, $f_{\rm sat}$.

4.1 Evolution models

In this discussion, all methods are defined in reference to an N-body simulation which follows the evolution of clustering of the dark matter. The models we compare, along with the labels used to refer to these models in the subsequent discussion, are as follows.

Fixed number density. This is the model discussed in the previous sections, using the output from SAMs. At each redshift, samples are constructed by ranking galaxies in order of descending stellar mass. Galaxies are retained down to the stellar mass which allows the sample to attain the desired number density. This procedure is repeated anew at each redshift, without any consideration of the galaxies included in samples at other redshifts. There can be considerable churn in the galaxies which make up a sample defined by a fixed number density at different redshifts. Galaxies may merge, and so no longer exist as a distinct entity at a subsequent redshift. Differences in star formation rates between galaxies mean that some galaxies may not gain stellar mass as quickly as others and so may lose their place on the list of galaxies that make up the sample at a later redshift, being replaced by a galaxy that was not previously included. So, although the number density of the sample does not change with redshift, the membership of the sample is not fixed (see further discussion in Section 4.2).

Tracking evolution. The tracking model follows the same galaxy population across time. In this case, the galaxy samples are defined at a specified redshift as described above, by ranking in order of decreasing stellar mass and retaining all the galaxies down to a particular mass to achieve a given number density. This exact sample of galaxies is then followed using the SAM implemented in the N-body simulation. The size of the sample can shrink as galaxies merge according to the treatment of galaxy mergers in the SAM. Note that at a subsequent redshift, the sample of galaxies in the tracking evolution model can differ substantially from the fixed number density sample outlined above. This is because the galaxies in the tracking evolution case are not necessarily the most massive at a redshift subsequent to the one at which the sample is defined. Different tracking evolution samples can be defined by changing the redshift at which the sample is initially specified. Star formation is effectively ignored after the redshift at which the sample is defined since the sample membership is not reconsidered, but it provides a somewhat idealized way probing galaxy evolution by tracking an identical set of galaxies over time.

Passive evolution. The passive evolution model imposes strict assumptions regarding the physical 'passivity' of the galaxies, following an unchanged galaxy population. The starting point is again the output of the SAM in the N-body simulation at a specified redshift, selecting all galaxies above a specific stellar mass to reproduce a set number density. The passive evolution model differs from the tracking evolution model in that the number of objects is preserved. If, according to the SAM, two galaxies merge, the remnant galaxy counts twice in the HOD, effectively doubling the weight of the remnant in any clustering prediction. Again, star formation is ignored after the redshift at which the sample is defined. In such a passive evolution, each galaxy keeps its own identity and there is no merging or disruption of satellites or formation of new ones. Such strong assumptions lend themselves to theoretical predictions of the evolution and empirical comparisons (e.g. Fry 1996; White et al. 2007; Guo & White 2014; Skibba et al. 2014). A detailed study of the evolution of clustering and the HOD under passive evolution was presented by Seo et al. (2008).

Descendant clustering selection. This method was proposed by Padilla et al. (2010) to investigate the clustering of the descendants of a population of galaxies observed at $z > 0$. As before, our starting point is the output of the SAM model at a particular redshift. The aim is to select a sample of dark matter haloes that has the same clustering as the galaxy sample: in the original method the galaxy sample in question was an observational sample, here it is the output of the SAM ranked by stellar mass. The clustering of the galaxy sample is characterized in terms of the median host halo mass. A sample of dark matter haloes is then constructed with the same median

mass, starting from the most massive haloes in the simulation and giving each halo equal weight (so effectively $\langle N(M_h)\rangle = 1$). These haloes are then followed in the simulation and their evolved median halo mass is used to identify descendants of the original sample (again ranked by stellar mass). The underlying assumption is that no objects enter or leave the sample between the selection redshift and the redshift at which the descendants are considered but mergers can take place. The number of descendant haloes can be smaller than the number at the selection redshift following mergers between haloes.

4.2 Comparison of results

In Fig. 11, we compare the ratio $M_1/M_{\rm min}$ (top panel) and the satellite fraction (bottom panel) obtained for the different evolution models set out above. The heuristic models are defined using different selection samples taken from the G13 model, varying the selection redshift using a space density of $n = 6.56 \times 10^{-3}\,h^3\,{\rm Mpc}^{-3}$. The black solid line in each panel shows the value of these quantities for the fixed number density extracted from the output of the SAMs at each redshift. The predictions of the other models are shown for different definition redshifts, which correspond to the redshifts at which the other line colours and styles branch off the black line.

The predictions of the alternative evolution models shown in Fig. 11 for the evolution of the $M_1/M_{\rm min}$ ratio and the satellites fraction are very different from the values measured in the SAM output for the fixed number density case. In particular, in the passive evolution model, satellite galaxies can only be accreted over time, but not destroyed. This leads to a dramatic increase of the satellite fraction with time (going towards smaller redshifts) and a decrease of the $M_1/M_{\rm min}$ ratio, in agreement with the conclusions reached by Seo et al. (2008). Thus, observing the opposite trend, as predicted by the SAMs for the fixed number density case, can serve as a clear diagnostic for non-passive evolution of the galaxies. The tracking model, in which satellites accrete and merge over time while no new galaxies enter the evolving sample, results in a shallower increase of the satellite fraction and a shallower decline of the characteristic masses ratio. The descendants model predictions for the $M_1/M_{\rm min}$ ratio are similar to the passive evolution one, while the satellite fraction decreases with time. These trends are due to the descendants model producing a lower number density at $z = 0$ than the higher redshift starting one, which leads to generally decreasing with time satellite fractions and $M_1/M_{\rm min}$ values.

In all the alternative models, the ratio $M_1/M_{\rm min}$ is predicted to decline with time following the selection redshift, as shown in Fig. 11, whereas for the fixed number density samples in the SAM output this ratio increases by ∼50 per cent by the present day, over the redshift interval plotted. This, again, highlights the importance of this diagnostic in deciphering among different evolution scenarios.

The predictions of the empirical models for the satellite fraction can diverge in either direction away from the SAM output, to both higher and lower values. The reason that the passive evolution model predicts a substantially larger number of satellites than is seen in the SAM model output (and as a consequence, a lower value of $M_1/M_{\rm min}$) is because galaxy mergers are not allowed in this model, which preserves the number of galaxies. However, halo mergers do take place with the consequence that central galaxies are converted into satellite galaxies when their host halo merges with a more massive halo. Even with galaxy mergers occurring in the case of the fixed number density evolution, it appears that the balance is towards converting centrals to satellites, such that the satellite fraction increases mildly with time. This trend is also in accordance with observational estimates (e.g. Zheng et al. 2007; Coupon et al. 2012; Skibba et al. 2015).

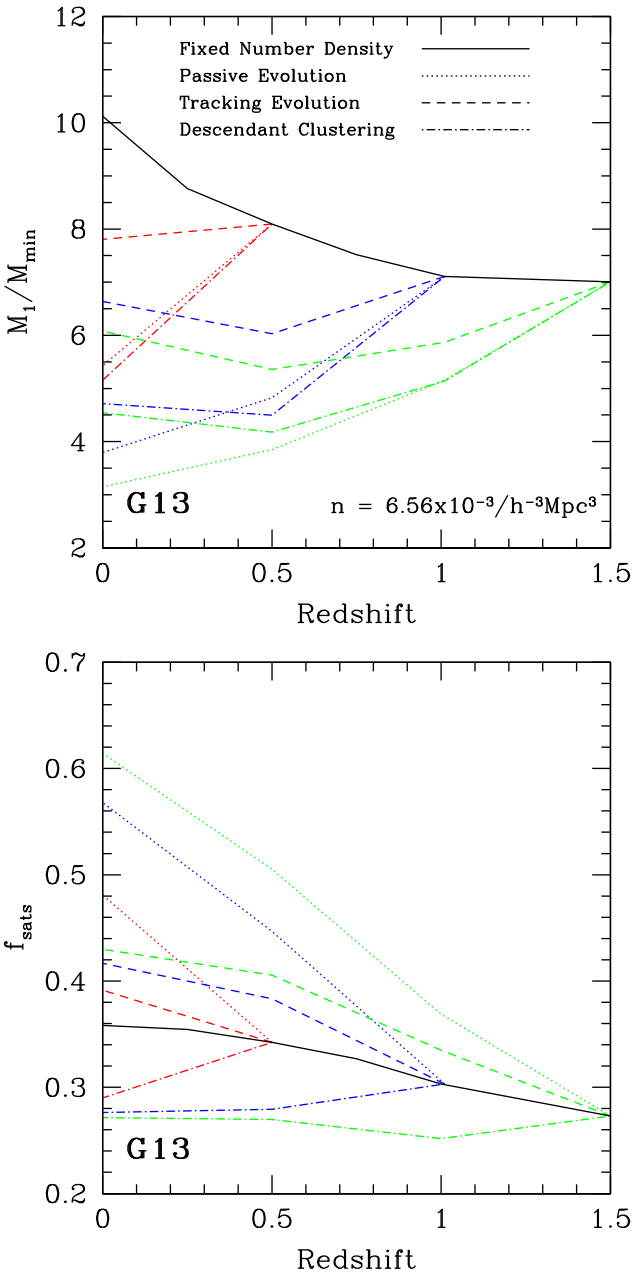

Figure 11. The evolution of the $M_1/M_{\rm min}$ ratio (top) and the satellite fraction, $f_{\rm sat}$, (bottom) in the G13 model for the fixed number density sample of $6.56 \times 10^{-3}\,h^3\,{\rm Mpc}^{-3}$ (solid black lines). The other lines show the predictions of the alternative heuristic models discussed in the text, for different choices of the selection redshift (i.e. where they start departing from the solid black line): passive evolution (dotted lines), tracking evolution (dashed lines) and descendant clustering evolution (dash–dotted lines). The colours indicate the redshift at which these models are defined: $z = 0.5$ (red), 1 (blue) and 1.5 (green).

Another major difference between the evolution of the fixed number density samples and the passive and tracking models is the significant change in the identity of the galaxies in the sample in the former case. The change goes much beyond compensating for the galaxy mergers that occur over time. A large number of galaxies enter and leave the sample essentially due to galaxy evolution, namely

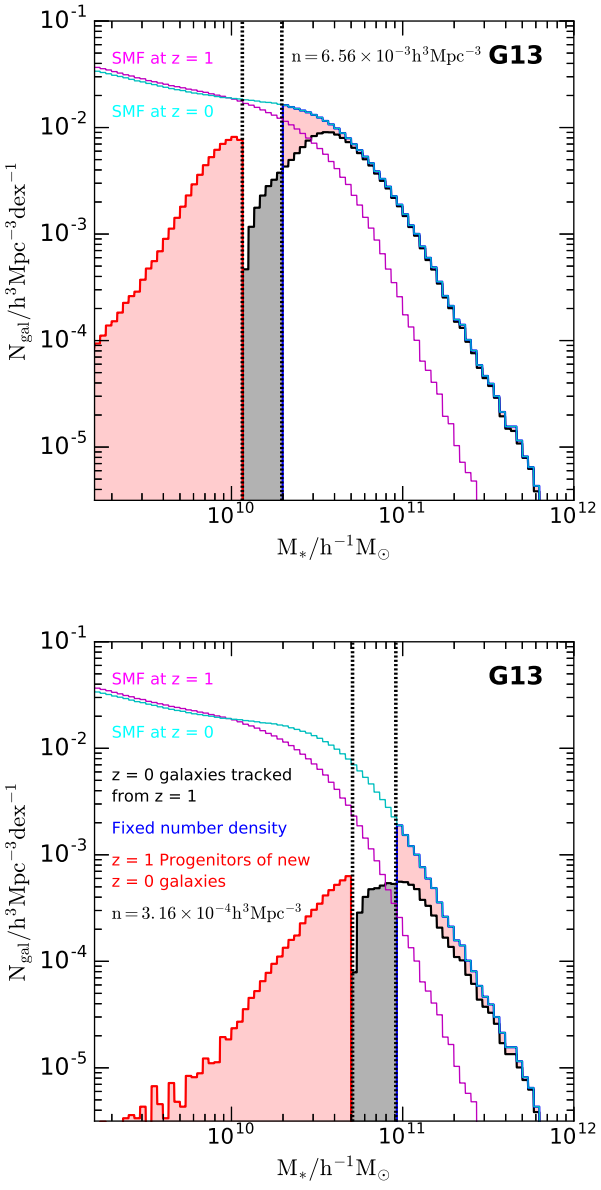

Figure 12. The changing membership of stellar-mass-selected samples in the G13 model, for a number density of $6.56 \times 10^{-3}\,h^{-3}\,\mathrm{Mpc}^3$ (top) and $n = 3.16 \times 10^{-4}\,h^3\,\mathrm{Mpc}^{-3}$ (bottom). The overall stellar mass function is shown for $z = 0$ (cyan) and $z = 1$ (magenta). The black-dashed vertical lines show the cut in stellar mass for the number density sample at $z = 1$ (leftmost line) and $z = 0$ (rightmost line). The blue solid line histogram represents the stellar mass distribution of galaxies that make up the stated fixed number density sample at $z = 0$ (rightmost histogram line). The black solid line histogram shows the galaxies at $z = 0$, whose progenitors consisted of the fixed number density sample at $z = 1$ (middle histogram line). The white region in common of these two histograms represents the galaxies who remained in the sample from $z = 1$ to 0, while the grey shaded area represents the descendants of the galaxies that were in the sample at $z = 1$ but are no longer members at $z = 0$ (middle shaded area). Also, conversely, many progenitors of the galaxies that are in the sample at $z = 0$ were not members at $z = 1$. These are denoted by the shaded pink areas (rightmost and leftmost shaded areas), where the red line histogram shows their distribution at $z = 1$ (leftmost histogram line), and the shaded pink region under the blue histogram shows their stellar mass at $z = 0$. These galaxies compensate for both the grey region galaxies that fell out of the sample due to stunted stellar mass growth and for the galaxies that were destroyed due to merging since $z = 1$.

Table 5. Evolution of the galaxy samples identity from $z = 1$ to 0 for two representative number densities, $n = 6.56 \times 10^{-3}\,h^{-3}$ Mpc and $n = 3.16 \times 10^{-4}\,h^{-3}\mathrm{Mpc}^3$, in the G13 SAM. This table shows the percentage of galaxies at $z = 1$ that exit the sample during the redshift interval and those that entered the sample to maintain the constant number of galaxy members. The difference in the percentage of galaxies that 'enter' and 'exit' the sample is equal to the percentage of galaxies that underwent a merger in that time frame. The columns are 'total galaxies' representing the full galaxy sample and 'satellite galaxies', representing the percentage (of the total number of galaxies in the sample at $z = 1$) of galaxies that are satellites (i.e. the percentage that are central galaxies equals 'total galaxies' minus 'satellite galaxies' numbers).

$n/h^{-3}\mathrm{Mpc}^3$	Status	Total galaxies	Satellite galaxies
6.56×10^{-3}	Exit	8	5
6.56×10^{-3}	Enter	33	10
3.16×10^{-4}	Exit	34	13
3.16×10^{-4}	Enter	55	13

differences in the star formation rates or growth of stellar mass, that result in changed ranking of the galaxies by stellar mass (Leja et al. 2013; Mundy et al. 2015; Torrey et al. 2015).

To illustrate how the membership of the sample changes with redshift, we show in Fig. 12 the evolution in stellar mass between $z = 1$ and 0 for two representative fixed number density samples in the G13 SAM. The galaxies under the histogram that is shaded grey were originally members of the sample defined by number density at $z = 1$, but are no longer part of a sample defined by the same number density at $z = 0$. These galaxies are no longer the most massive, but instead have been replaced by the galaxies which, at $z = 1$, corresponded to those shaded pink under the red histogram. These galaxies were not massive enough to be included in the sample at $z = 1$ but grew in mass more quickly than some of the galaxies which were in the sample, hence replacing them when the sample was redefined in terms of the number density of the most massive galaxies when ranked by stellar mass at $z = 0$. These promoted galaxies are shown in pink shading under the blue histogram. (Note when comparing the areas under the curves that this is a log–log plot.) The new galaxies that entered the sample since $z = 1$ compensate for both the ones that fell out of the sample due to stunted stellar mass growth and the ones that got destroyed by mergers.

These changes in the sample identity are in fact quite significant. Table 5 provides the percentage of galaxies that exit and enter these two fixed number density samples between $z = 1$ and 0. The difference between the galaxies that enter and leave is equal to the number of galaxies that merge with other members of the sample. For the $n = 6.56 \times 10^{-3}\,h^{-3}$ Mpc sample, 8 per cent of the galaxies exit the sample between $z = 1$ and 0 and about a third of the sample are new galaxies that entered. The turn in membership is even more prominent for lower number densities (more massive galaxies), and for the $n = 3.16 \times 10^{-4}\,h^{-3}\mathrm{Mpc}^3$ sample about a third of the galaxies exit and more than half of the galaxies enter the sample over that redshift interval.

These changes in the sample identity also impact the number of central and satellite galaxies, though the more significant factor is the balance between accretion and destruction of satellites within the sample. That is, satellite galaxies which merge with their central galaxies tend to be replaced by central galaxies (whose stellar mass growth rate is typically larger than satellites that experience quenching). However, the dominant effect seems to be the halo mergers

turning central galaxies into satellites, resulting in an overall slight increase of the satellite fraction with time.

5 SUMMARY AND CONCLUSIONS

The HOD framework has proven to be a useful theoretical tool to interpret galaxy clustering measurements and describe the relation between galaxies and dark matter haloes. Here, we set to study how the halo occupation models evolve with time, an aspect that is missing from standard applications, using the outputs of SAMs that capture the galaxy formation physics. It is important to recall that the SAMs predict the galaxy content of dark matter haloes along with the properties of these galaxies. The halo occupation functions are used here as a useful approach to characterize how the haloes are populated by galaxies in the SAMs. The halo occupation function has the attraction that it can be readily written in terms of the contribution from the main (e.g. most luminous or the galaxy from the most massive progenitor halo) or central galaxy, and satellite galaxies, which were once central galaxies in their host haloes but have subsequently merged with more massive dark matter haloes. Furthermore, the halo occupation function in itself is not dependent on the radial distribution of galaxies within haloes (though an assumption about this is required to predict the correlation function from the HOD). This is appealing for our purposes, as different SAMs handle the placement of galaxies within haloes in different ways (see the discussion in Contreras et al. 2013 and Campbell et al. 2015).

The SAMs we consider use different implementations of the physical processes involved in galaxy formation and set the values of the model parameters in different ways, putting emphasis on different observables (Henriques et al. 2015; Lacey et al. 2016). We compare the model output at a series of number densities for galaxies ranked by their stellar mass. (Note that we also show the stellar mass functions so the reader can see how closely these agree with one another.) The HODs look remarkably similar until the samples characterized by the lowest number densities. In this case, the details of the suppression of gas cooling by heating by accretion on to active galactic nuclei become important and introduce differences in the HOD of central galaxies.

The main aim for this study is to characterize the evolution of the HOD at a fixed number density, and we explore the evolution of the HOD best-fitting parameters over the redshift range $0 \leq z \leq 3$. As always, it is important to first assess which features of the SAMs are robust to the details of the implementation of the physics and the setting of the model parameters. Four out of the five parameters in the HOD parametrization that we used displayed remarkably similar behaviour. As before, this similarity was strained when comparing the lowest density samples or the parameter which describes the transition from zero to one galaxy for the central HOD.

Three of the HOD parameters are masses (see Fig. 1 for an illustration of how the parameters control the shape of the HOD). The evolution of the best-fitting values of these masses for samples of fixed number density is much weaker than the evolution in the characteristic halo mass (roughly speaking the mass at which there is a break from a power law in the halo mass function). We found that the evolution is well described by a single parameter describing a power law in redshift and the $z = 0$ value of the parameter.

We also compared the evolution predicted in the SAMs to simplified evolution models that have been used to model galaxy clustering and evolution. These models make different assumptions about the fate of 'galaxies' identified at some redshift. None of these models behave in the same way as the output of the SAMs, giving very different predictions for the evolution of the HOD parameters and the fraction of satellite galaxies in the sample. We find, in particular, that the ratio between the characteristic halo mass for hosting a satellite galaxy to that of hosting a central galaxy and its change with redshift can serve as a sensitive diagnostic for different galaxy formation and evolution scenarios.

In so far as the models describe the clustering of stellar mass selected samples and its evolution, our results can be used to build mock catalogues for surveys from $z = 0$ to 3. Typically, an observational determination of the HOD may exist for one redshift, e.g. the low-redshift results for *r*-band-selected galaxies from Zehavi et al. (2011). The problem becomes how to extend these best-fitting parameters to other redshifts where there may not be an equivalent determination of the HOD parameters. For example, one might want to build a mock catalogue for the *Euclid* redshift survey, which will recover emission line galaxies over the redshift range $z \approx 0.5$–2 from a measurement of the clustering of Hα emitters at a different redshift (e.g. Geach et al. 2012). We plan to pursue such efforts in future work.

ACKNOWLEDGEMENTS

This work was made possible by the efforts of Gerard Lemson and colleagues at the German Astronomical Virtual Observatory in setting up the Millennium Simulation data base in Garching, and John Helly and Lydia Heck in setting up the mirror at Durham. We thank Zheng Zheng and Hong Guo for many useful discussions. We thank the referee for insightful comments that improved the presentation of the paper. SC and IZ acknowledge the hospitality of the ICC at Durham and the helpful conversations with many of its members. We acknowledge support from the European Commission's Framework Programme 7, through the Marie Curie International Research Staff Exchange Scheme LACEGAL (PIRSES-GA-2010-269264) and from an STFC/Newton Fund award (ST/M007995/1). SC further acknowledges support from CONICYT Doctoral Fellowship Programme. IZ is supported by NSF grant AST-1612085, as well as by a CWRU ACES+ ADVANCE Opportunity Grant and a Faculty Seed Grant. IZ and PN acknowledge support from the European Research Council, through the ERC Starting Grant DEGAS-259586. IZ, CMB and PN additionally acknowledge the support of the Science and Technology Facilities Council (ST/L00075X/1). CMB acknowledges a research fellowship from the Leverhume Trust. NP is supported by 'Centro de Astronomıa y Tecnologıas Afines' BASAL PFB-06 and by Fondecyt Regular 1150300. PN further acknowledges the support of the Royal Society through the award of a University Research Fellowship. The calculations for this paper were performed on the ICC Cosmology Machine, which is part of the DiRAC-2 Facility jointly funded by STFC, the Large Facilities Capital Fund of BIS and Durham University, and on the Geryon computer at the Center for Astro-Engineering UC, part of the BASAL PFB-06, which received additional funding from QUIMAL 130008 and Fondequip AIC-57 for upgrades.

REFERENCES

Abbas U. et al., 2010, MNRAS, 406, 1306
Baugh C. M., 2006, Rep. Prog. Phys., 69, 3101
Behroozi P. S., Conroy C., Wechsler R. H., 2010, ApJ, 717, 379
Benson A. J., 2010, Phys. Rep., 495, 33
Benson A. J., Cole S., Frenk C. S., Baugh C. M., Lacey C. G., 2000, MNRAS, 311, 793
Berlind A. A., Weinberg D. H., 2002, ApJ, 575, 587

Berlind A. A. et al., 2003, ApJ, 593, 1
Blake C., Collister A., Lahav O., 2008, MNRAS, 385, 1257
Bower R. G., Benson A. J., Malbon R., Helly J. C., Frenk C. S., Baugh C. M., Cole S., Lacey C. G., 2006, MNRAS, 370, 645
Brown M. J. I. et al., 2008, ApJ, 682, 937
Bullock J. S., Wechsler R. H., Somerville R. S., 2002, MNRAS, 329, 246
Campbell D. J. R. et al., 2015, MNRAS, 452, 852
Cole S., Lacey C. G., Baugh C. M., Frenk C. S., 2000, MNRAS, 319, 168
Conroy C., Wechsler R. H., Kravtsov A. V., 2006, ApJ, 647, 201
Contreras S., Baugh C. M., Norberg P., Padilla N., 2013, MNRAS, 432, 2717
Contreras S., Baugh C. M., Norberg P., Padilla N., 2015, MNRAS, 452, 1861
Cooray A., 2006, MNRAS, 365, 842
Cooray A., Sheth R., 2002, Phys. Rep., 372, 1
Coupon J. et al., 2012, A&A, 542, A5
Coupon J. et al., 2015, MNRAS, 449, 1352
Croton D. J. et al., 2006, MNRAS, 365, 11
Croton D. J. et al., 2016, ApJS, 222, 22
Davis M., Efstathiou G., Frenk C. S., White S. D. M., 1985, ApJ, 292, 371
de la Torre S. et al., 2013, A&A, 557, A54
De Lucia G., Blaizot J., 2007, MNRAS, 375, 2
De Lucia G., Kauffmann G., White S. D. M., 2004, MNRAS, 349, 1101
Durkalec A. et al., 2015, A&A, 583, A128
Eisenstein D. J. et al., 2011, AJ, 142, 72
Font A. S. et al., 2008, MNRAS, 289, 1619
Fontanot F., De Lucia G., Monaco P., Somerville R. S., Santini P., 2009, MNRAS, 397, 1776
Fry J. N., 1996, ApJ, 461, L65
Geach J. E., Sobral D., Hickox R. C., Wake D. A., Smail I., Best P. N., Baugh C. M., Stott J. P., 2012, MNRAS, 426, 679
Gonzalez-Perez V., Lacey C. G., Baugh C. M., Lagos C. D. P., Helly J., Campbell D. J. R., Mitchell P. D., 2014, MNRAS, 439, 264 (GP14)
Guo Q., White S., 2014, MNRAS, 437, 3228
Guo Q. et al., 2011, MNRAS, 413, 101
Guo Q., White S., Angulo R. E., Henriques B., Lemson G., Boylan-Kolchin M., Thomas P., Short C., 2013, MNRAS, 428, 1351 (G13)
Guo H. et al., 2014, MNRAS, 441, 2398
Guo H. et al., 2015a, MNRAS, 446, 578
Guo H. et al., 2015b, MNRAS, 453, 4368
Hamana T., Yamada T., Ouchi M., Iwata I., Kodama T., 2006, MNRAS, 369, 1929
Hearin A. P., Zentner A. R., van den Bosch F. C., Campbell D., Tollerud E., 2016, MNRAS, 460, 2552
Henriques B. M. B., White S. D. M., Thomas P. A., Angulo R. E., Guo Q., Lemson G., Springel V., 2013, MNRAS, 431, 3373
Henriques B. M. B., White S. D. M., Thomas P. A., Angulo R., Guo Q., Lemson G., Springel V., Overzier R., 2015, MNRAS, 451, 2663
Jiang L., Helly J. C., Cole S., Frenk C. S., 2014, MNRAS, 440, 2115
Jing Y. P., Börner G., 1998, ApJ, 503, 37
Jing Y. P., Mo H. J., Börner G., 1998, ApJ, 494, 1
Jing Y. P., Börner G., Suto Y., 2002, ApJ, 564, 15
Kim H.-S., Baugh C. M., Cole S., Frenk C. S., Benson A. J., 2009, MNRAS, 400, 1527
Kim J.-W., Im M., Lee S.-K., Edge A. C., Wake D. A., Merson A. I., Jeon Y., 2015, ApJ, 806, 189
Krause E., Hirata C. M., Martin C., Neill J. D., Wyder T. K., 2013, MNRAS, 428, 2548
Kravtsov A. V., Berlind A. A., Wechsler R. H., Klypin A. A., Gottlöber S., Allgood B., Primack J. R., 2004, ApJ, 609, 35
Lacey C. G. et al., 2016, MNRAS, 462, 3854
Lagos C. D. P., Baugh C. M., Lacey C. G., Benson A. J., Kim H.-S., Power C., 2011, MNRAS, 418, 1649
Lagos C. D. P., Bayet E., Baugh C. M., Lacey C. G., Bell T. A., Fanidakis N., Geach J. E., 2012, MNRAS, 426, 2142
Lee K.-S., Giavalisco M., Gnedin O. Y., Somerville R. S., Ferguson H. C., Dickinson M., Ouchi M., 2006, ApJ, 642, 63
Lee K.-S., Giavalisco M., Conroy C., Wechsler R. H., Ferguson H. C., Somerville R. S., Dickinson M. E., Urry C. M., 2009, ApJ, 695, 368
Leja J. et al., 2013, ApJ, 778, L24
McCracken H. J. et al., 2015, MNRAS, 449, 901
Magliocchetti M., Porciani C., 2003, MNRAS, 346, 186
Manera M. et al., 2015, MNRAS, 447, 437
Merson A. I. et al., 2013, MNRAS, 429, 556
Moustakas L. A., Somerville R. S., 2002, ApJ, 577, 1
Mundy C. J., Conselice C. J., Ownsworth J. R., 2015, MNRAS, 450, 3696
Padilla N. D., Christlein D., Gawiser E., González R. E., Guaita L., Infante L., 2010, MNRAS, 409, 184
Padilla N. D., Salazar-Albornoz S., Contreras S., Cora S. A., Ruiz A. N., 2014, MNRAS, 443, 2801
Parejko J. K. et al., 2013, MNRAS, 429, 98
Peacock J. A., Smith R. E., 2000, MNRAS, 318, 1144
Phleps S., Peacock J. A., Meisenheimer K., Wolf C., 2006, A&A, 457, 145
Quadri R. F., Williams R. J., Lee K.-S., Franx M., van Dokkum P., Brammer G. B., 2008, ApJ, 685, L1
Rodríguez-Puebla A., Behroozi P., Primack J., Klypin A., Lee C., Hellinger D., 2016, MNRAS, 462, 893
Ross A. J., Percival W. J., Brunner R. J., 2010, MNRAS, 407, 420
Scoccimarro R., Feldman H. A., Fry J. N., Frieman J. A., 2001, ApJ, 546, 652
Seljak U., 2000, MNRAS, 318, 203
Seo H.-J., Eisenstein D. J., Zehavi I., 2008, ApJ, 681, 998
Simon P., Hetterscheidt M., Wolf C., Meisenheimer K., Hildebrandt H., Schneider P., Schirmer M., Erben T., 2009, MNRAS, 398, 807
Skibba R. A. et al., 2014, ApJ, 784, 128
Skibba R. A. et al., 2015, ApJ, 807, 152
Somerville R. S., Davé R., 2015, ARA&A, 53, 51
Springel V., White S. D. M., Tormen G., Kauffmann G., 2001, MNRAS, 328, 726
Springel V. et al., 2005, Nature, 435, 629
Torrey P. et al., 2015, MNRAS, 454, 2770
van den Bosch F. C., Yang X., Mo H. J., 2003, MNRAS, 340, 771
Wake D. A. et al., 2008, MNRAS, 387, 1045
Wake D. A. et al., 2011, ApJ, 728, 46
Watson D. F., Berlind A. A., Zentner A. R., 2011, ApJ, 738, 22
White M., Zheng Z., Brown M. J. I., Dey A., Jannuzi B. T., 2007, ApJ, 655, L69
White M. et al., 2011, ApJ, 728, 126
Yan R., Madgwick D. S., White M., 2003, ApJ, 598, 848
Yang X., Mo H. J., van den Bosch F. C., 2003, MNRAS, 339, 1057
Yang X., Mo H. J., Jing Y. P., van den Bosch F. C., 2005, MNRAS, 358, 217
Zehavi I. et al., 2005, ApJ, 630, 1
Zehavi I. et al., 2011, ApJ, 736, 59
Zentner A. R., Berlind A. A., Bullock J. S., Kravtsov A. V., Wechsler R. H., 2005, ApJ, 624, 505
Zheng Z., 2004, ApJ, 610, 61
Zheng Z., Guo H., 2016, MNRAS, 458, 4015
Zheng Z. et al., 2005, ApJ, 633, 791
Zheng Z., Coil A. L., Zehavi I., 2007, ApJ, 667, 760
Zheng Z., Zehavi I., Eisenstein D. J., Weinberg D. H., Jing Y. P., 2009, ApJ, 707, 554

This paper has been typeset from a TEX/LATEX file prepared by the author.